Chapter 3

Study of synchrotron power losses in tokamak plasmas

3.1   Introduction

Synchrotron losses are usually estimated in system studies, with expressions derived from a plasma description using simplifying assumptions on the geometry, radiation absorption, and density and temperature profiles. The use of these approximate expressions can be explained both by the small magnitude of the synchrotron radiation losses in present tokamaks and by the complexity of the exact calculation. As synchrotron losses become significant in the power balance of high temperature plasmas envisaged for a steady state commercial reactor (see Chapter 6), it is time to propose a complete formulation of the transport of synchrotron radiation performed for realistic conditions of toroidal plasma geometry with elongated cross-section, using an accurate method for the calculation of the absorption coefficients, and for arbitrary shapes of density and temperature profiles.

The effects of toroidicity and temperature profile on synchrotron radiation losses are analysed in detail. In particular, when the electron temperature profile is almost flat in the plasma centre as, for example, in internal transport barrier confinement regimes, synchrotron losses are found to be much stronger than in the case where the profile is represented by its best generalized parabolic approximation, though both cases give approximately the same thermal energy content. Such an effect is not included in presently used approximate expressions.

Finally, considering the quantitative importance of the new effects introduced in our analysis, we propose a seven variable fit for the fast calculation of synchrotron radiation losses. This fit is derived from a large database, which has been generated using a code implementing the complete formulation, and optimized for massively parallel computing.

3.2 Physics issues

3.2.1 Electron cyclotron frequency

The synchrotron radiation has its origin in the gyromotion of the electrons around the magnetic field lines confining the plasma. The trajectory of these electrons is determined by the Lorentz force of motion

$$\mathbf{F} = \frac{d\mathbf{p}_e}{dt} = e\left(\mathbf{v} \times \mathbf{B}\right), \tag{3.1}$$

where $\mathbf{p}_e$ is the electron momentum and e is the absolute charge of the electron. The magnetic field in a tokamak is the resultant of the superposition of two independent components: the toroidal magnetic field and the poloidal magnetic field. The latter one is perpendicular to and much smaller than the toroidal magnetic field $\mathbf{B}_t$. Hence, only $\mathbf{B}_t$ is considered in the calculation of the electron synchrotron radiation.
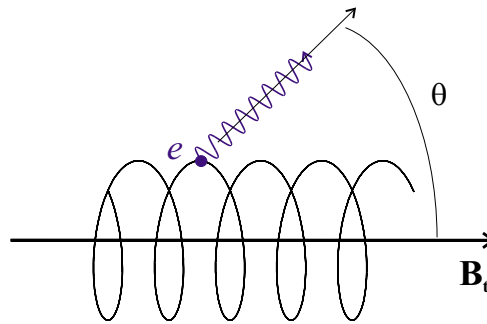

Figure 3.1: Synchrotron motion and emission of an electron turning around a magnetic field line $\mathbf{B}_t$

In the non-relativistic limit ($v \ll c$), Eq. (3.1) may be solved as a uniform rotation with frequency

$$\omega_{ce} = \frac{e}{m_e}B_t, \tag{3.2}$$

combined with a uniform translation. Here ω_{ce} is the electron cyclotron frequency and m_e is the electron mass.

The electromagnetic wave emitted by an electron moving with a velocity $\mathbf{v}$ and a frequency ω_{ce} is periodic but not simply harmonic, due to the relativistic effects included in Maxwell's equations. Hence, it could be thought that the electron emits and absorbs electromagnetic waves at the cyclotron frequency ω_{ce} and its harmonics n, i.e. $\omega = n\omega_{ce}$ with ($n = 1, 2, 3, ...$). Nevertheless, the relativistic dynamics modify the frequency ω at which the electron emits and absorb waves, due to the

relativistic electron mass effect and to the Doppler effect [Bor83]. For a wave vector **k**, it can be then written that

$$\omega = \frac{n\omega_{ce}}{\gamma} + k_\parallel v_\parallel$$

with

$$\gamma = \frac{1}{\sqrt{1 - (v/c)^2}}, \tag{3.3}$$

and the $k_\parallel v_\parallel$ term describes the parallel Doppler effect.

3.2.2 Radiation emission in the absence of absorption

In the non-relativistic case, the total power radiated by a single electron in the vacuum [Jac75] is given by the Larmor's formula

$$P_{e_0} = \frac{e^2}{6\pi\epsilon_0 c^3}\left(\frac{dv}{dt}\right)^2. \tag{3.4}$$

In the presence of a magnetic field B_t and assuming a Maxwellian distribution for the electrons, with a density n_e and temperature T_e, the synchrotron radiation power emitted "in vacuum" per unit of volume is expressed from Eqs (3.1) and (3.4) as

$$\frac{dP_{e_0}}{dV} = \frac{\omega_{ce}^2\omega_{pe}^2}{3\pi c^3}kT_e, \tag{3.5}$$

where c is the speed of light and ω_{pe} is the electron plasma frequency, which is defined as

$$\omega_{pe}^2 = \frac{e^2}{\epsilon_0 m_e}n_e. \tag{3.6}$$

In the relativistic case, an individual electron moving in a magnetic field along a spiral line emits the following energy taking into account the contribution of all harmonics

$$P_{e_{0,\gamma}} = \frac{e^2}{6\pi\epsilon_0 c^3}\omega_{ce}^2\frac{v_\perp^2}{\gamma^2}. \tag{3.7}$$

Integrating Eq. (3.7) for a Maxwellian relativistic distribution for the electrons:

$$f = \frac{\mu\exp\left(-\mu\gamma\right)}{4\pi K_2\left(\mu\right)} \tag{3.8}$$

with $\mu = m_e c^2/kT_e$, the total emission per unit of plasma volume in the absence of absorption, and in the relativistic case, can be derived in closed from [Tru58], i.e.

$$\frac{dP_{e_{0,\gamma}}}{dV} = \frac{\omega_{ce}^2\omega_{pe}^2}{3\pi c^3}kT_e\frac{K_3\left(\mu\right)}{K_2\left(\mu\right)}, \tag{3.9}$$
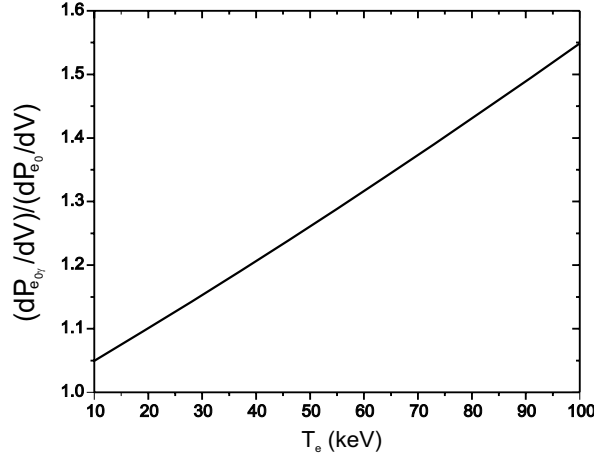
Figure 3.2: Ratio of vacuum emission power in the relativistic case to the non-relativistic case versus the temperature, for a homogeneous plasma with $\omega_{ce}/2\pi = 190$ GHz and $\omega_{pe}/2\pi = 83$ GHz (corresponding to $B_t \simeq 6.8$ T and $n_e \simeq 0.85 \times 10^{20}$ m^{-3}).

where $K_\nu(\mu)$ are modified Bessel functions of the second kind (also called MacDonald functions) and $\mu = m_e c^2/(kT_e)$. Note that in the non-relativistic case ($\gamma \to 1$, $\mu \to \infty$) Eq. (3.9) reduces to Eq. (3.5).

Fig. 3.2 compares the total vacuum emission taking into account the relativistic effects or not, for a temperature interval of 10 to 100 keV.

3.2.3   The radiative transfer equation

The transport of synchrotron radiation is characterized by the specific intensity J_ω, defined as the synchrotron radiation power per unit of solid angle, unit of surface normal to the direction of propagation and unit of frequency ω. In a tokamak plasma, J_ω, which depends on the local competition between the emission and absorption phenomena, is a function of local properties such as temperature and refractive index.

When all these quantities are known, the specific intensity can be deduced from the following equation of radiative transfer [Bek66]:

$$N_{r,\omega}^2 \frac{d}{d\sigma}\left(\frac{J_\omega}{N_{r,\omega}^2}\right) = \eta_\omega - \alpha_\omega J_\omega, \qquad (3.10)$$

where σ is the co-ordinate along the ray path, $N_{r,\omega}$ is the radiation refractive index, α_ω is the absorption coefficient and η_ω is the emissivity of the plasma, i.e. the power radiated away per unit of volume, solid angle and frequency. For frequencies for
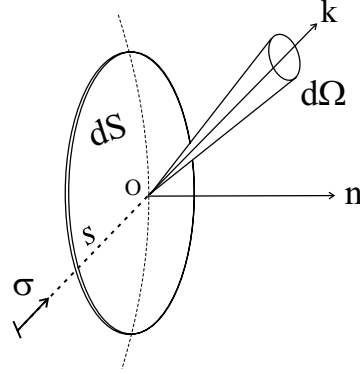
Figure 3.3: Vector diagram for a ray path of length s crossing the area dS corresponding to the exit point O of the plasma.

which the synchrotron loss is not negligible ($\omega^2/\omega_{pe}^2 \gg 1$), the ray path can be approximated by a straight line. This approximation will be used throughout this study.

One of the difficulties in the problem of synchrotron radiation transport is the calculation of the absorption coefficients at each point of the plasma, for all frequencies and all ray path directions (see Section 3.2.4). The absorption coefficient and the emissivity of a plasma in thermodynamic equilibrium are related locally by Kirchoff's law, which for tokamak plasmas ($\hbar\omega \ll kT_e$), is appropriately described by the Rayleigh-Jeans approximation:

$$\frac{1}{N_{r,\omega}^2}\frac{\eta_\omega}{\alpha_\omega} = \frac{\omega^2}{8\pi^3 c^2} kT_e. \tag{3.11}$$

The integration of Eq. (3.10) over a ray path of length s, whose origin and end are placed on the entry and exit points of the plasma, respectively ($N_{r,\omega}^2(0) = N_{r,\omega}^2(s) = 1$), yields an exponential expression describing the self-absorption of the radiation:

$$J_\omega(s) = J_\omega(0)\exp\left(-\int_0^s \alpha_\omega \, d\sigma\right)$$
$$+ \frac{\omega^2}{8\pi^3 c^2} k \int_0^s T_e(\sigma)\,\alpha_\omega(\sigma)\exp\left(-\int_\sigma^s \alpha_\omega(\sigma')\,d\sigma'\right) d\sigma. \tag{3.12}$$

In the particular case of no reflecting walls around the plasma, we have $J_\omega(0) = 0$. Introducing the non-dimensional optical thickness τ as

$$\tau = \int_0^s \alpha_\omega \, d\sigma,$$

the plasma is said to be optically thick when $\tau \gg 1$. In this case, the plasma emits like a blackbody. On the contrary, the plasma is said to be optically thin when $\tau \ll 1$, in which case the self-absorption is negligible.

3.2.4 Radiation absorption by the plasma

The electromagnetic properties of the plasma are determined from Maxwell's equations through the conduction current density $\mathbf{j}$ and the space charge density ρ. The source terms $\mathbf{j}$ and ρ, in turn, are determined by the microscopic motions of the particles under the action of internal and external forces. The response to these forces is given by the linearized kinetic equation (or Boltzmann equation). Combining this equation with Maxwell equations, a set of wave equations describing the propagation of the electric field $\mathbf{E}$ are obtained. The resulting equations can be Fourier analysed considering the electric field to be made up locally of a superposition of plane waves (i.e. $\propto \exp\left(j\omega t - i\mathbf{k} \cdot \mathbf{r}\right)$):

$$\mathbf{k} \times (\mathbf{k} \times \mathbf{E}) + \left(\frac{\omega}{c}\right)^2 \boldsymbol{\epsilon} \cdot \mathbf{E} = 0, \tag{3.13}$$

where $\mathbf{k}$ is the wave vector and $\boldsymbol{\epsilon}$ is the plasma dielectric tensor defined from the Ohm's law as:

$$\boldsymbol{\epsilon} = 1 + \frac{1}{i\omega\epsilon_0}\frac{\mathbf{j}}{\mathbf{E}}.$$

The quantity $\boldsymbol{\epsilon}$ determines the response of the plasma to the electromagnetic field and therefore describes the physics of the problem. Eq. (3.13) leads to a set of linear and homogeneous equations for three orthogonal electric field components. The condition for the existence of a non-trivial solution is that the determinant Λ of the coefficients of the electric field $\mathbf{E}$ vanishes, i.e. $\Lambda = 0$. This is the so-called dispersion relation, which relates the frequency ω and the wave vector $\mathbf{k}$ or refractive index, i.e. $\mathbf{N} = \left(\frac{c}{\omega}\right)\mathbf{k}$.

In the orthogonal frame of reference with the magnetic field along the $\mathbf{z}$ axis direction and assuming the wave vector $\mathbf{k}$ propagating in the $\mathbf{x} - \mathbf{z}$ plane, as shown in Fig.3.4, the general form of the dispersion relation is found to be:

$$\Lambda = \begin{vmatrix} \epsilon_{xx} - N_\parallel^2 & \epsilon_{xy} & \epsilon_{xz} + N_\perp N_\parallel \\ \epsilon_{yx} & \epsilon_{yy} - \left(N_\perp^2 + N_\parallel^2\right) & \epsilon_{yz} \\ \epsilon_{zx} + N_\perp N_\parallel & \epsilon_{zy} & \epsilon_{zz} - N_\perp^2 \end{vmatrix} = 0, \tag{3.14}$$

Each solution of the dispersion relation is a characteristic mode of oscillation that the plasma is able to propagate.

Expressing the components of the dielectric tensor as a sum of harmonics by means of Bessel functions $J_n(z)$, the general expression for the components of the
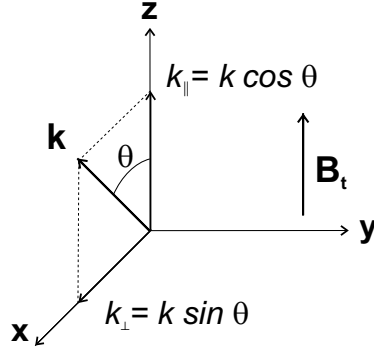
Figure 3.4: Magnetic field $\mathbf{B}_t$ and wave vector $\mathbf{k}$ in the orthogonal (x, y, z) frame.

plasma dielectric tensor for an isotropic distribution function f may be written as [Gra91]

$$\epsilon_{jl} = \delta_{jl} + \frac{\omega_{pe}^2}{\omega^2} \sum_{n=-\infty}^{n=\infty} n^2 \int \frac{1}{u} \frac{df}{du} \frac{u_\perp^2 \Pi_{jn}^* \Pi_{ln}}{\rho^2 \left(\gamma - n\omega_{ce}/\omega - k_\parallel u_\parallel c/\omega \right)} d\mathbf{u}$$

with $j, l = x, y, z$ and

$$\mathbf{u} = \mathbf{p}_e / \left(m_e c \right), \quad \rho = \frac{N_\perp u_\perp}{Y_1}, \quad Y_n = \frac{n\omega_{ce}}{\omega},$$

$$\Pi_{1n} = J_n \left(\rho \right), \quad \Pi_{2n} = -i \frac{\rho J_n' \left(\rho \right)}{n}, \quad \Pi_{3n} = \frac{N_\perp u_\parallel J_n \left(\rho \right)}{Y_n}$$

with $J_n' \left(\rho \right) = dJ_n / d\rho$. Taking for the electrons a Maxwellian relativistic distribution f (Eq. (3.8)), we obtain the following components of the dielectric tensor:

$$\epsilon_{jl} = \delta_{jl} + \frac{\mu^2}{4\pi K_2 \left(\mu \right)} \frac{\omega_{pe}^2}{\omega^2} \sum_{n=-\infty}^{n=\infty} n^2 \int \frac{u_\perp^2 \Pi_{jn}^* \Pi_{ln} \exp \left(-\mu\gamma \right)}{\gamma \rho^2 \left(\gamma - n\omega_{ce}/\omega - k_\parallel u_\parallel c/\omega \right)} d\mathbf{u}, \quad (3.15)$$

which obey the additional symmetry relations

$$\epsilon_{xy} = -\epsilon_{yx}, \quad \epsilon_{yz} = -\epsilon_{zy}, \quad \epsilon_{xz} = \epsilon_{zx}.$$

They can be split into an Hermitian ϵ_{jl}' and an anti-Hermitian ϵ_{jl}'' part for a convenient calculation,

$$\epsilon_{jl} = \epsilon_{jl}' + i\epsilon_{jl}''. \quad (3.16)$$

In the range of parameters of interest for the synchrotron losses problem ($\omega > 2\omega_{ce}$), the Hermitian part of the dielectric tensor is well described by the cold plasma approximation in the high frequency limit (Appleton-Hartree equation).

For the calculation of the anti-Hermitian part of the dielectric tensor, thermal and relativistic effects need to be retained. Practical expressions for the anti-Hermitian and Hermitian parts are reported in Appendix B.

The absorption coefficient: The absorption coefficient α_ω may be deduced from the rate of decay of the electromagnetic wave. Hence, noting that the wave intensity I (as well as the wave energy) is proportional to the square of the modulus of the electric field ($I \propto |\mathbf{E}|^2$), the exponential decrease in the intensity is specified by twice the imaginary part of the wave vector $\mathbf{k}$,

$$I \propto \exp\left[-2\mathbf{r}\operatorname{Im}\left(\mathbf{k}\right)\right].$$

Assuming a weak absorption ($\operatorname{Im} k \ll \operatorname{Re} k$), which is indeed the only case where the wave propagation is effectively possible, the absorption coefficient is given by

$$\alpha_\omega^{(i)} = -2\left|\operatorname{Im}\left(\mathbf{k}\right)\right|. \tag{3.17}$$

In this equation, the absorption coefficient α_ω refers to a specific fundamental wave mode (i) corresponding to one solution of the dispersion relation.

3.3   Global synchrotron power losses and transparency factor

The explicit expression for the global synchrotron power lost through the plasma surface is obtained by integrating the specific intensity on the exit point of the plasma $J_\omega(s)$ over the plasma surface S, frequencies ω, and solid angles Ω corresponding to the external hemisphere

$$P_{\mathrm{syn},S} = \int_\omega d\omega \int_\Omega d\Omega \int_S J_\omega\, \mathbf{k} \cdot \mathbf{dS}, \tag{3.18}$$

where $\mathbf{k}$ is the direction of the ray path. Using $\mathbf{dS} = \mathbf{N}dS$, Eq. (3.18) may be expressed as

$$P_{\mathrm{syn},S} = \int_\omega d\omega \int_S dS \int_\Omega J_\omega \cos(\mathbf{k}, \mathbf{N})d\Omega. \tag{3.19}$$

As seen in Fig. 3.5, in the presence of wall reflections around the plasma surface, a fraction r (called the reflection coefficient) of $P_{\mathrm{syn},S}$ is reflected towards the plasma, resulting in a new absorption phase which modifies J_ω at each point of the plasma surface and for all directions. The part which is effectively lost (denoted as P_{syn}) is that going through the walls, i.e.

$$P_{\mathrm{syn}} = (1 - r)\, P_{\mathrm{syn},S}.$$

In the present study, we analyse the synchrotron radiation losses in the absence of wall reflections (the corresponding losses are denoted as P_{syn_0}). In this case, the
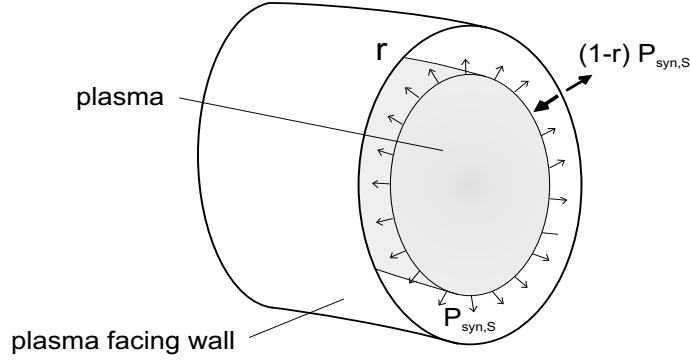
Figure 3.5: Schematic diagram of synchrotron power losses in the presence of wall reflections.

specific intensity on the entry point of the plasma is $J_\omega(0) = 0$ (see Eq. (3.12)), and we have $P_{\mathrm{syn}_0} = P_{\mathrm{syn},S}$. Although the effect of wall reflections is not treated in this study, a fair estimation of such an effect can be made using the correction factor obtained in Ref. [Tru79] for cylindrical plasmas:

$$P_{\mathrm{syn}} = (1-r)^{1/2} P_{\mathrm{syn}_0}.\tag{3.20}$$

This correction factor has been checked in Ref. [Tam88] to be found to be valid also in the case of toroidal plasma geometry.

For a convenient calculation, the synchrotron power loss P_{syn} is usually expressed in a dimensionless form. Here P_{syn} is normalized to the source of synchrotron radiation P_{e_0}, obtained by integrating the non-relativistic Larmor formula (Eq. (3.5)) over a homogeneous plasma cylinder of finite length $2\pi R$ (where R is the major radius) with a circular cross-section of minor radius a

$$P_{e_0} = 2\pi^2 a^2 R \frac{\omega_{pe}^2 \omega_{ce}^2}{3\pi c^3} kT_e.\tag{3.21}$$

The resulting dimensionless parameter

$$\Phi^* = P_{\mathrm{syn}}/P_{e_0}\tag{3.22}$$

reduces to the real transparency factor Φ (fraction of the total emission which is effectively lost), in the case of a homogeneous plasma cylinder with circular cross-section in the non-relativistic limit. In this study, Φ^* will be called the transparency factor parameter.

Note that, for present tokamak plasmas as well as for the next step and commercial reactors, the synchrotron radiation ($f_c = n\omega_{ce}/2\pi$) is predominantly emitted in

the millimetre or sub-millimetre range ($30 < f_c < 3000$ GHz). For such frequencies, the effective radiation absorption by the plasma itself results in transparency factors of the order of a few percents ($0.1 < \Phi < 5\%$) [Bor83], so that $\Phi \ll 1$.

It can be easily shown that in the absence of self-absorption of the synchrotron emission magnetic confinement fusion would not be feasible. As an illustration, the synchrotron radiation power emitted in the absence of self-absorption in a D-T commercial reactor plasma is typically of $10 - 20$ GW.

3.4 Review of synchrotron loss studies

The above formulation for the transport of synchrotron radiation was first proposed by Trubnikov [Tru58] and by Drummond and Rosenbluth [Dru63] for homogeneous plasmas with slab and circular cylinder geometries. Using several approximations, including a first order saddle-point method for the calculation of the absorption coefficients, Trubnikov [Tru79] derived a simple fit for the calculation of the global loss due to synchrotron radiation in the temperature range 10-100 keV, for a homogeneous plasma cylinder with circular cross-section:

$$P_{\mathrm{syn}_0(\mathrm{TRU})} = 8.20 \times 10^{-10} R a^{3/2} T_e^{5/2} B_{t_0}^{5/2} n_e^{1/2}. \tag{3.23}$$

In this work, the additional effect of the inhomogeneity of the magnetic field due to toroidal geometry is described using the approximate correction factor

$$(1 + \chi(\varepsilon, T_e))^{1/2}$$

with

$$\chi(\varepsilon, T_e) \simeq 18 \frac{\varepsilon}{T_e^{1/2}} \quad \text{and} \quad \varepsilon = a/R.$$

In system studies, the calculation of synchrotron losses in a tokamak plasma is still generally performed using the above Trubnikov's fit.

A comparable fit was derived by Tamor [Tam83] for homogeneous plasmas with slab geometry and temperatures in the range 100-1000 keV, using an exact absorption coefficient and taking into account the relativistic effects on the vacuum emission (Eq. (3.9)).

An exhaustive review of synchrotron loss studies for a homogeneous plasma with cylindrical geometry and circular cross-section was presented by Bornatici et al. [Bor83]. In this review, a comparison is presented between Trubnikov's fit and a complete calculation using the saddle-point formalism to all orders for the calculation of the absorption coefficients. A reasonable agreement is found in the temperature range 20-30 keV, for plasma parameters characteristic of present day tokamaks as well as for plasma parameters relevant for reactors with high magnetic fields and finite wall reflection coefficients.

In the case of inhomogeneous plasmas with toroidal geometry, Tamor [Tam88] uses a Monte Carlo code where a large number of rays are tracked throughout the plasma. This method allows a rigorous analysis of wall reflections and, associated with a radial discretization, gives access to the energy redistribution on the plasma profile, but it is much more demanding in computation time than the method described above. In his work, Tamor compares the complete numerical calculation of synchrotron losses, with the volume integration of a power loss density obtained by dividing the Trubnikov total power loss by the plasma volume and considering the result as a local quantity. For a circular plasma cross-section, with a central temperature of 50 keV, an acceptable agreement is found for both flat and parabolic profiles. It is, however, important to note that this approach of a local character of the Trubnikov calculation has no rigorous justification.

Finally, corrections to the Trubnikov's fit in the range of temperatures of D-T tokamak plasmas have been proposed by Fidone et al. [Fid92]

$$P_{\mathrm{syn}_0(\mathrm{FMGG})} = 8.20 \times 10^{-10} R a^{3/2} E_1(\kappa) \ \langle T_e \rangle^{5/2} B_{t_0}^{5/2} \langle n_e \rangle^{1/2}$$

$$\times \frac{(1 + \alpha_n)^{1/2} (1 + \alpha_T)^{5/2}}{\left(1 + \frac{1}{2}\alpha_n + \frac{5}{2}\alpha_T\right)} (1 + \chi(\varepsilon, T_e))^{\frac{1}{2}}, \qquad (3.24)$$

taking into account the ellipticity of the plasma cross-section through $E_1(\kappa) = \frac{2}{\pi}\kappa E[(1 - 1/\kappa^2)^{1/2}]$, where $E(x)$ is the complete elliptic integral of the second kind, and the inhomogeneity of density and temperature, both described with generalized parabolic profiles as follows:

$$n_e = n_{e_0} \left(1 - \rho^2\right)^{\alpha_n}, \quad T_e = T_{e_0} \left(1 - \rho^2\right)^{\alpha_T}, \qquad (3.25)$$

where n_{e_0} and T_{e_0} are the density and temperature at the magnetic axis, α_n and α_T are the density and temperature peaking parameters and ρ is the normalized radius ($\langle n_e \rangle$ and $\langle T_e \rangle$ are the volume average density and temperature, respectively). Let us notice that the function $E_1(\kappa)$ is the unity for circular cross-sections ($\kappa = 1$).

The latter expression for the calculation of synchrotron losses will be referred to as the FMGG fit.

3.5   Synchrotron losses in cylindrical plasmas

In a first stage we develop the formalism of synchrotron radiation losses for cylindrical palsmas of finite length $L = 2\pi R$, being R the major radius of the simulated torus.

3.5.1 Homogeneous plasma with circular cross-section

We consider a circular cross-section of radius a, without wall reflections, and with flat profiles for density and temperature distributions. The magnetic field is considered to be homogeneous in the whole plasma and equal to its value at the magnetic axis $B_t = B_{t_0}$, so that the radiation source is uniformly distributed over the plasma volume.
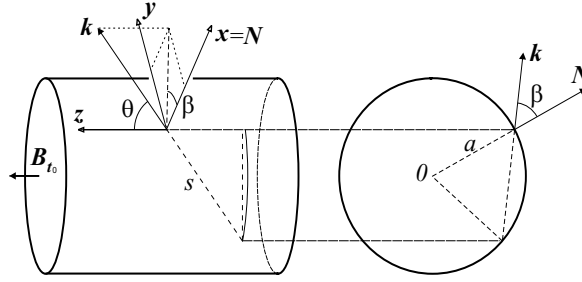

Figure 3.6: Geometrical parameters for the calculation of synchrotron losses in a plasma cylinder with circular cross-section.

In this special case of a homogeneous and isotropic environment, i.e. η_ω and α_ω independent from σ, Eq. (3.12) yields to a simple expression for the specific intensity per unit of frequency:

$$J_\omega = \frac{\omega^2}{8\pi^3 c^2} kT_e \left[1 - \exp\left(-s\alpha_\omega\right)\right], \tag{3.26}$$

and normalizing the global synchrotron power losses (Eq. (3.19)) crossing the surface $S = 2\pi a L$ by the vacuum emission in the non-relativistic limit (Eq. (3.21)), we obtain the following explicit expression for the transparency factor parameter per unit of frequency:

$$\Phi_\omega^* = \frac{3}{4\pi^2 p_a} \frac{\omega^2}{\omega_{ce}^3} \int_\Omega \left[1 - \exp\left(-s\alpha_\omega\right)\right] \cos(\mathbf{k}, \mathbf{N}) d\Omega, \tag{3.27}$$

where p_a is a dimensionless parameter called the opacity factor:

$$p_a = \frac{a\omega_{pe}^2}{c\omega_{ce}}. \tag{3.28}$$

Using the above assumptions and according to the plasma geometry illustrated in Fig. 3.6, the integration over the solid angles Ω may be expressed as a function of the angle θ between the direction of the ray path and the magnetic field, and the

angle β between the projection of the ray path on the plane perpendicular to the magnetic field and the normal to the cylinder surface, as

$$\int_\Omega d\Omega = 2 \int_0^\pi \sin\theta d\theta \int_0^{\frac{\pi}{2}} d\beta,$$

as well as

$$\cos(\mathbf{k}, \mathbf{N}) = \sin\theta \cos\beta.$$

This latter expression is valid for any plasma geometry (circular or elliptical cross-section, cylindrical or toroidal geometry). The length of the ray path s may then be expressed as

$$s = 2a\frac{\cos\beta}{\sin\theta},$$

and Eq. (3.27) becomes

$$\Phi_\omega^* = \frac{3}{2\pi^2 p_a} \frac{\omega^2}{\omega_{ce}^3} \int_0^\pi \sin^2\theta d\theta \int_0^{\frac{\pi}{2}} \cos\beta \left[1 - \exp\left(-2a\frac{\cos\beta}{\sin\theta}\alpha\right)\right] d\beta. \quad (3.29)$$

Introducing $\nu = \omega/\omega_{ce}$, the transparency factor parameter Φ_ν^* per unit of normalized frequency is defined as $\Phi_\nu^* = \omega_{ce}\Phi_\omega^*$, and provided that the absorption coefficient α_ω is calculated differently for the ordinary (o) and extraordinary (x) mode of propagation and for each frequency ($\alpha_\omega^{(i)}$), the total transparency factor parameter can be written as

$$\Phi^* = \frac{3}{2\pi^2 p_a} \sum_{i=o,x} \left[\int_0^\infty \nu^2 d\nu \int_0^{\pi/2} \sin^2\theta d\theta \right.$$

$$\left. \times \int_{-\pi/2}^{\pi/2} \cos\beta \left[1 - \exp\left(-2a\alpha_\nu^{(i)}\frac{\cos\beta}{\sin\theta}\right)\right] d\beta \right]. \quad (3.30)$$

For a practical computation of Eq. (3.30), the integration over normalized frequencies ν in the interval $\nu = [0, \infty[$, may be avoided by introducing the variable ν_1,

$$\nu = \frac{1}{\nu_1} - 1 \quad \text{with} \quad d\nu = -\frac{d\nu_1}{\nu_1^2}, \quad (3.31)$$

so that the integration is then performed over the interval $\nu_1 = [0, 1]$.

3.5.2 Trubnikov's method for the calculation of the absorption coefficients

For a simple calculation of the absorption coefficients, Trubnikov [Tru79] proposes an approximation using the following assumptions. First of all, the synchrotron radiation is supposed to be emitted at high enough harmonics for the density

effect on the real part of the wave vector to be negligible ($\mathrm{Re}\,(N) = 1$). Secondly, the absorption coefficients are derived for all directions by neglecting a term which is small only if the direction of propagation is almost perpendicular to the magnetic field (where the absorption is indeed maximum). Next, the Bessel functions which appear in the components of the dielectric tensor are asymptotically expanded for weakly relativistic plasmas ($kT_e \ll m_e c^2$). Finally, the evaluation of the integrals involved in the calculation of the components of the dielectric tensor is performed using a saddle-point technique, for which Trubnikov retains only the first saddle-point.

In fact, Drummond and Rosenbluth [Dru63] and De Barbieri [Bar77] have shown the existence of an infinite number of saddle-points. Keeping the first one is a good approximation only in the high frequency limit ($\omega/\omega_{ce} \gg m_e c^2/kT_e$). Note that this condition is much more restrictive for low temperatures ($T_e < 20$ keV), for which the synchrotron radiation is also mainly emitted at relatively low harmonics ($\omega/\omega_{ce} < 10$).

With the above method, which will be referred to as the Trubnikov's approximate method, the magnetic field and the electron density appear to be grouped within the dimensionless parameter p_a. In Section 3.6 we investigate whether this approximate method is or not applicable in plasmas interesting for nuclear fusion.

Trubnikov's approximate method yields the following expressions of the absorption coefficients $\alpha_\nu^{(i)}(p_a, t, \theta, \nu)$ for the ($i = o, x$) mode of propagation and normalized frequency ν [Tru79]:

$$a\alpha_\nu^{(i)} \simeq \left(\frac{\pi}{2}\right)^{1/2} p_a \left(\frac{t}{\tau f}\right)^{1/2} \sin^3\theta \frac{\lambda_i}{(f^2 - \cos^2\theta)^{3/2}}$$

$$\times \exp\left\{-\frac{1}{t}\left[\frac{1}{\sin\theta}(f^2 - \cos^2\theta)^{1/2} - 1\right]\right\}, \qquad (3.32)$$

$$\begin{cases} \lambda_o = (1 + \frac{f}{t}\cos^2\theta)(f^2 - \cos^2\theta)^{1/2} + \frac{\cos^2\theta}{t\sin\theta} \\ \lambda_x = (1 + \frac{f}{t})(f^2 - \cos^2\theta)^{1/2} + \frac{f^2}{t\sin\theta} \end{cases}$$

and

$$f(\tau) = (\cosh y - 1)\tau \qquad (3.33)$$

with

$$\sinh y - y = \frac{1}{\tau} \quad \text{and} \quad \tau = t\nu\sin^2\theta.$$

In the above expressions, t is the normalized temperature ($t = kT_e/m_e c^2$) and θ is the angle between the direction of the ray and the magnetic field.

A fast evaluation of the function $f(\tau)$ has been implemented using asymptotic expansions for small and large values of τ, and approximations by Chebychev poly-

nomials for the intermediate values. For $\tau < 0.01$, the following asymptotic expansion for $\tau \to 0$ is used:

$$f(\tau) = 1 - \tau \ln \tau - (1 - \ln 2)\tau - \tau^2 \ln \tau$$
$$+ \left(\ln 2 + \frac{1}{2} \right) \tau^2 + \tau^2 \varepsilon(\tau). \tag{3.34}$$

For $\tau \geq 10.6$, we use the following asymptotic expansion for large τ:

$$f(\tau) = \frac{3^{2/3}}{2^{1/3}} \tau^{1/3} + \frac{3^{4/3}}{5 \times 2^{5/3}} \frac{1}{\tau^{1/3}} - \frac{27}{1400} \frac{1}{\tau} + O\left(\frac{1}{\tau^{5/3}} \right). \tag{3.35}$$

Finally, in the intervals $[0.01 - 0.1[$, $[0.1 - 0.5[$, $[0.5 - 1.6[$, $[1.6 - 4.3[$, and $[4.3 - 10.6[$, five order Chebychev expansions are derived using numerical solution of Eq. (3.33).

The precision of the resulting approximation is better than 7×10^{-5} for $0 < \tau < \infty$.

3.5.3 Reproducing the Trubnikov's calculation

Trubnikov's study for the calculation of the synchrotron losses in a tokamak plasma considers both the set of geometric and profile assumptions detailed in Section 3.5.1 (i.e. cylindrical homogeneous plasma with circular cross-section), and the method for the calculation of the absorption coefficients detailed in Section 3.5.2. The Trubnikov's fit (Eq. 3.23), which is still used in system studies, is deduced from the numerical calculations made by Trubnikov with this model.

Fig. 3.7 compares the transparency factor parameters as reported by Trubnikov and those resulting from the numerical integration of Eq. (3.30) with $\alpha_\nu^{(i)}$ given by Eqs (3.32) and (3.33), using exactly the same set of assumptions. Differences of 0-30% are observed for the main parameters range for the synchrotron losses problem.

Let us reproduce the fit for the calculation of synchrotron losses in the absence of reflection walls for a cylindrical homogeneous plasma with circular cross-section, using two dimensionless fitting variables: the normalized temperature t and the opacity factor parameter p_a. We take the same parameter ranges as those considered by Trubnikov for deducing his fit. That is a temperature range $5 - 100 \, \text{keV}$ and a p_a range[1] $10^2 - 10^5$.

From a dataset made of 225 numerical calculations with a relative error which is taken to be lower than 10^{-4}, we obtain the following fit:

$$\Phi^*_{\text{circular}(A \to \infty)} = 83 t^{1.37} p_a^{-0.54}$$

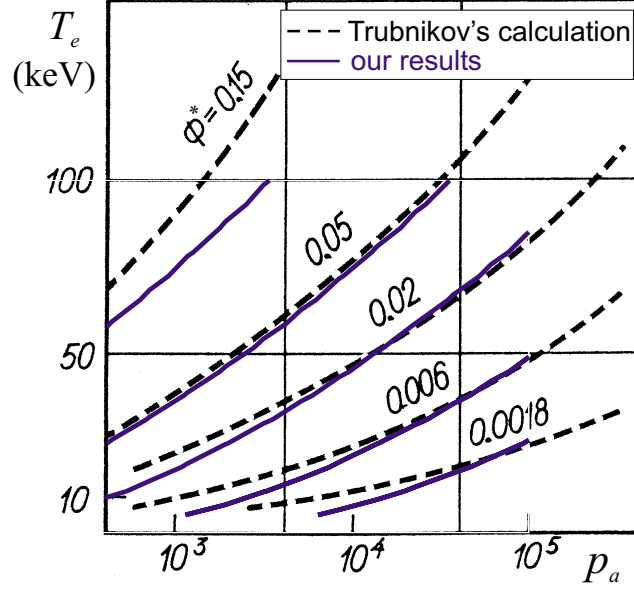[1] The p_a interval is divided in equal-logarithmic parts.

Figure 3.7: Comparison of the transparency factor contours in the (p_a, T_e) plane provided by Trubnikov computations with our results.

with a RMSE $\simeq 25\%$. This expression is not very different from Trubnikov's fit (Eq. 3.23) which, using the dimensionless parameters t and p_a, can be expressed as

$$\Phi^*_{\text{TRU}} = 60 t^{1.5} p_a^{-0.5}$$

with RMSE $\simeq 50\%$ [Tru72].

3.5.4 Elliptical plasma cross-section: extension of Trubnikov's fit

A more realistic elliptical plasma cross-section, with elongation κ, is now considered. As seen in the cylindrical geometry illustrated in Fig. 3.8, the integration over the solid angles Ω is not symmetrical with respect to positive and negative angles β,

$$\int_\Omega d\Omega = \int_0^\pi \sin\theta \, d\theta \int_{-\frac{\pi}{2}}^{\frac{\pi}{2}} d\beta$$

The surface of a cylindrical plasma with elliptical cross section is given by:

$$\int_S dS = 2\pi a R \int_0^{2\pi} (\sin^2\varphi + \kappa^2 \cos^2\varphi)^{1/2} d\varphi. \tag{3.36}$$
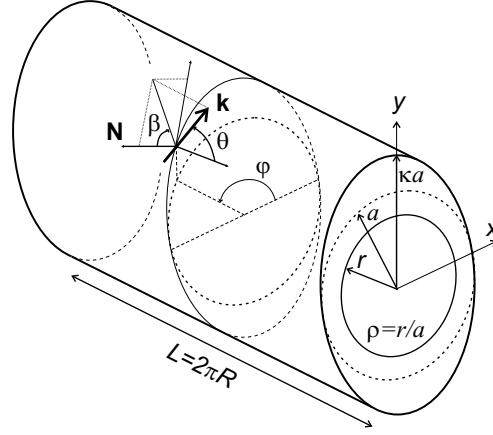
63

Figure 3.8: Geometrical parameters for the calculation of synchrotron losses in a cylindrical plasma with elliptical cross-section.

Note that the right-hand integral can be expressed as $2\pi E_1(\kappa)$, where $E_1(\kappa) = \frac{2}{\pi}\kappa E[(1 - 1/\kappa^2)^{1/2}]$.

In a similar way to the circular case, the length of the ray path s may be expressed as

$$s = 2as^{\star}\frac{\cos\beta}{\sin\theta}$$

with $s^{\star} = s^{\star}(\kappa, \varphi, \beta)$,

$$s^{\star} = \frac{\kappa(\sin^2\varphi + \kappa^2\cos^2\varphi)^{3/2}}{\kappa^2\sin^2\beta - 2\kappa(\kappa^2 - 1)\sin\varphi\cos\varphi\sin\beta\cos\beta + (\sin^2\varphi + \kappa^4\cos^2\varphi)\cos^2\beta}. \tag{3.37}$$

With the above geometrical assumptions and assuming a homogeneous plasma (flat density, temperature, and magnetic field) with no wall reflections, the useful expression for the calculation of the transparency factor parameter Φ^* yields:

$$\Phi^* = \frac{3}{\pi^3 p_a}\sum_{i=o,x}\left[\int_0^{\infty}\nu^2 d\nu\int_0^{\pi/2}(\sin^2\varphi + \kappa^2\cos^2\varphi)^{1/2}d\varphi\int_0^{\pi/2}\sin^2\theta d\theta\right.$$

$$\left.\times\int_{-\pi/2}^{\pi/2}\cos\beta\left\{1 - \exp\left[-\frac{2a\alpha_{\omega}^{(i)}(\theta, \nu)}{\sin\theta}\cos\beta\,s^{\star}(\kappa, \varphi, \beta)\right]\right\}d\beta\right], \tag{3.38}$$

Note that there is a symmetry between the poloidal angle intervals $\varphi = [0, \pi/2]$ and $\varphi = [\pi/2, \pi]$. Introducing the variable $u = \frac{\sin\theta}{as^{\star}\cos\beta}\sigma$, the plasma normalized radius ρ is related to the integral variables σ, φ, θ and β, by

$$\rho^2 = 1 - Su\,(2 - u) \tag{3.39}$$

with

$$S\left(\kappa, \varphi, \beta\right) = \frac{\cos^2 \beta}{\kappa}(\sin^2 \varphi + \kappa^2 \cos^2 \varphi)^{1/2} s^\star(\kappa, \varphi, \beta). \qquad (3.40)$$

Trubnikov's fit for the calculation of synchrotron losses in cylindrical homogeneous plasmas has been extended to elliptical cross-sections, from a dataset made of 512 computations of Eq. (3.38) with the same temperature and p_a ranges[2] as those of the circular case (i.e. $5 - 100$ keV and $10^2 - 10^5$, respectively), and a κ range $1 - 2.5$. Taking an accuracy of numerical calculations lower than 10^{-4}, we obtain

$$\Phi^*_{\text{elliptic}(A\rightarrow\infty)} = 82t^{1.35}p_a^{-0.54}\kappa^{0.81}$$

with a RMSE $\simeq 28\%$. Let us notice that, when $\kappa = 1$, this expression almost reduces to the fit obtained in the circular case Φ^*_{circular}, which means the dependences of Φ^* on the normalized temperature t and opacity factor p_a are fairly independent from the value of the elongation κ. Other more subtle forms of elongation dependence have been tested, e.g. $\left(\frac{1+\kappa^2}{2}\right)^{x_1} \kappa^{x_2}$, giving similar t and p_a dependences and comparable RMSE indicators.

Fig. 3.9 shows the Φ^* dependence on κ calculated numerically using Eq. (3.38) with $\alpha_\nu^{(i)}$ given by Eqs (3.32) and (3.33). This dependence is compared in Fig. 3.9 with those obtained using the above fit $\Phi^*_{\text{elliptic}(A\rightarrow\infty)}$ and using the FMGG fit[3] (given by Eq. (3.24)), taking flat density and temperature profiles, and without taking into account the approximate correction factor describing the inhomogeneity of the magnetic field (i.e. $\Phi^*_{\text{FMGG}(A\rightarrow\infty)} = 60t^{1.5}p_a^{-0.5}E_1\left(\kappa\right)$).

Owing to the fact that the parameter Φ^* and the synchrotron power loss P_{syn_0} are related by the Larmor formula integrated over a homogeneous plasma cylinder with circular cross-section (Eq. (3.21)), the global synchrotron power loss P_{syn_0} has exactly the same κ dependence than that of the parameter Φ^*.

3.6 Comparison of the Trubnikov's method for the calculation of the absorption coefficients, with a quasi-exact method

In the present study, we propose a different method for the calculation of the absorption coefficients. This method uses a compact representation of the anti-Hermitian part of the dielectric tensor which has been proposed by Granata and Fidone [Gra91]. This formulation avoids the standard Larmor radius expansions of

---

[2]The p_a interval is divided in equal-logarithmic parts.

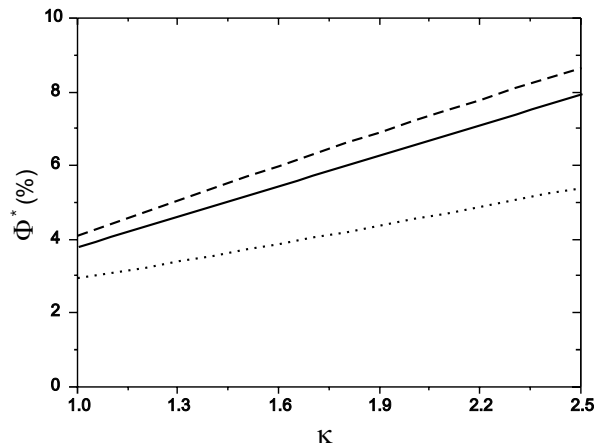[3]The FMGG fit keeps the same dependences on normalized temperature and opacity factor as Trubnikov's fit.

Figure 3.9: Comparison of the Φ^* parameter calculated numerically (solid line), calculated with the cylindrical fit (dashed line) and calculated wih the FMGG expression without the inhomogeneity of the magnetic field (dotted line), versus the elongation κ, for a homogeneous cylinder plasma with $p_a \simeq 3870$ and $T_e = 50$ keV.

Bessel functions (used, for example, by Tamor [Tam78]) and gives very accurate values, at least in the temperature range 10-50 keV, for all frequencies. When the ray path is parallel or almost parallel to the magnetic field, the value of Bessel functions appearing in this theory becomes undefined, in which case we use asymptotic expansions giving a precision better than 10^{-6} (see Appendix B for details). This formalism will be referred to as the quasi-exact method as opposed to Trubnikov's approximate method (described in Section 3.5.2).

Summarizing the differences between the two methods, the Trubnikov's approximate method:

- uses $\mathrm{Re}\,(N) = 1$,

- introduces an error for ray path directions not perpendicular to the magnetic field,

- is valid only for weakly relativistic plasmas in the high frequency limit;

whereas the quasi-exact method:

- uses a precise expression for the calculation of the real part of the refractive index (Appleton-Hartree equation),

- describes all ray path directions correctly,

66

- calculates the components of the dielectric tensor using a general representation which is valid for all the parameters of interest for the problem of synchrotron losses.

On the other hand, the Trubnikov's approach gives much lower computation times.

In Fig. 3.10, the Φ^* parameter per unit of normalized frequency is plotted for both methods using ITER-FDR parameters [FDR97] for flat electron temperatures of 10, 20, 30, 40 and 50 keV.
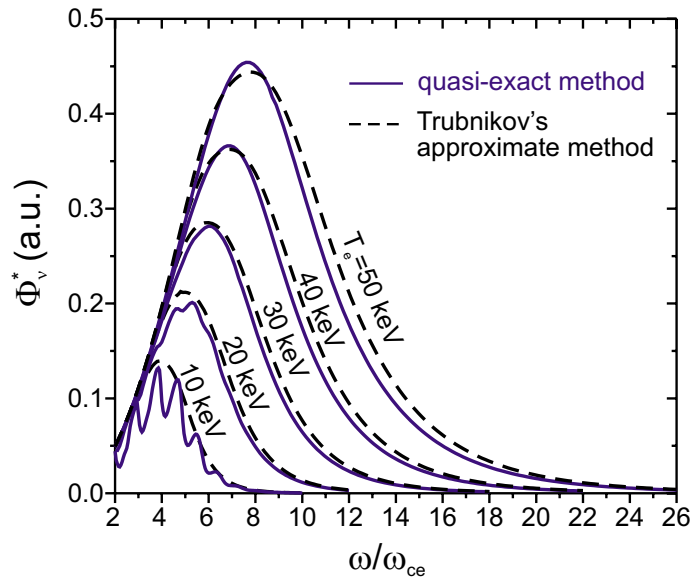

Figure 3.10: Transparency factor parameter versus normalized frequency for a circular plasma with flat profiles and an opacity factor $p_a \simeq 3870$, using Trubnikov's approximate method or the quasi-exact method for the calculation of the absorption coefficients.

We first note that Trubnikov's approximate method gives the correct asymptotic behaviour at very high frequencies for each temperature considered. On the other hand, this calculation produces a continuous spectrum because in the high frequency limit of the first order saddle-point approximation, the spectral lines overlap as a result of Doppler broadening. The quasi-exact method instead reproduces the spectral lines for low temperature and low frequencies.

Relative differences in the total Φ^* parameter, resulting from the numerical integration of Eq. (3.30) for each electron temperature, are presented in Table 3.1. Using Trubnikov's approach gives a 10% error with respect to the quasi-exact calculation

at electron temperatures of 20 keV, for which synchrotron losses are no longer negligible in the power balance of a tokamak plasma. The error keeps non-negligible values for higher temperatures.

Table 3.1: Relative difference between the total transparency factor parameters calculated using Trubnikov's approximate method and the quasi-exact one for different temperatures.

T_e (keV)	$\Phi^*_{\text{Trubnikov}}$ (%)	$\Phi^*_{\text{quasi-exact}}$ (%)	$\left(\dfrac{\Phi^*_{\text{quasi-exact}} - \Phi^*_{\text{Trubnikov}}}{\Phi^*_{\text{Trubnikov}}}\right) \times 100$
10	0.42	0.32	30.4
20	0.94	0.85	10.5
30	1.66	1.55	7.4
40	2.59	2.43	6.8
50	3.77	3.52	6.9

We conclude that Trubnikov's approximate method for the calculation of the absorption coefficients, though much faster than the quasi-exact method, also introduces non-negligible errors. To obtain accurate results for all plasma conditions, we will thus retain the quasi-exact method, leading to computation times which are reasonable with present day computers.

Similar relative differences are obtained for the entire opacity factor p_a range.

3.7 Spatial density of the synchrotron power loss in terms of emission

The spatial density of the synchrotron power loss in terms of emission dP_{em}/dV is the part of the synchrotron radiation power crossing the last magnetic surface which has been emitted in a given unit of plasma volume. With the aid of this spatial distribution, we can determine the plasma region that participates the most to the global loss due to the synchrotron radiation.

For clarity, let us specify that this spatial distribution dP_{em}/dV is not the local synchrotron power loss per unit volume dP_{syn}/dV (i.e. the difference between vacuum emission and absorption in the unit volume), which should be introduced, for example, in a 1D code for the self-consistent calculation of the temperature profile [Tam88]. Note however that both quantities integrated on the plasma volume give the same result.

3.7.1 Formulation of the problem

In order to treat the general problem of the synchrotron power crossing the last magnetic surface which has been emitted in an infinitesimal volume element dV (in the form of a pillbox in Fig. 3.11), we consider a ray path whose origin is placed on the entry point to the pillbox (separated a distance σ from the entry point 0 to the plasma), so that $J_\omega(\sigma) = 0$. Assuming the ray path to be a straight line, the radiation specific intensity dJ_ω leaving the pillbox within a solid angle $d\Omega$, is then given by Eq. (3.10):

$$dJ_\omega(\sigma) = \eta_\omega(\sigma)\, d\sigma, \tag{3.41}$$

where η_ω is the synchrotron emission power per unit of plasma volume dV in the spectral range $d\omega$ and per steradian flowing in the ray path direction. According to Kirchoff's law (Eq. (3.11)), it can be seen that

$$\eta_\omega(\sigma) = \frac{\omega^2}{8\pi^3 c^2} kT_e(\sigma)\ \alpha_\omega(\sigma)\,.$$
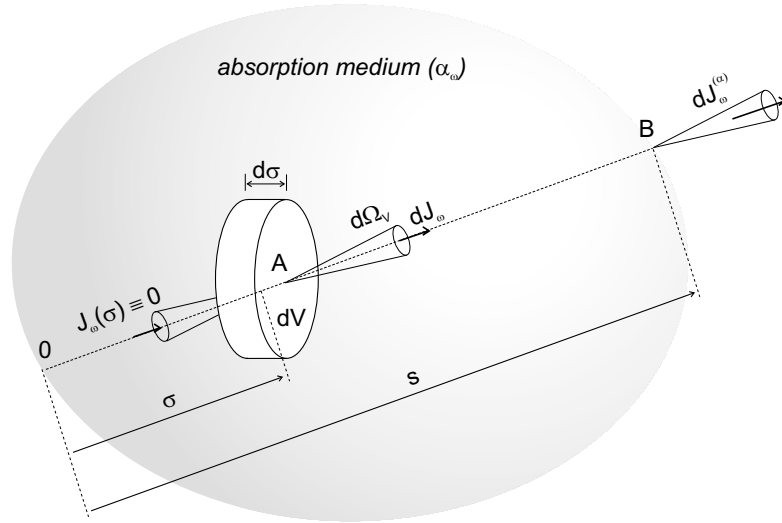

Figure 3.11: Radiation emitted in a small volume of plasma dV and leaving the medium after having suffered absorption.

From the point A to the exit point B of the plasma (throughout the plasma represented by an ellipsoid in Fig. 3.11), the medium is supposed only to absorb radiation (no emissivity, $\eta_\omega \equiv 0$). In this case and denoting the specific intensity of the radiation at the exit point of the absorbing plasma as $J_\omega^{(\alpha)}$, Eq. (3.10) leads to

$$J_\omega^{(\alpha)}(\text{B}) = J_\omega(\text{A}) \exp\left(-\int_\sigma^s \alpha_\omega\, d\sigma\right),$$

where s is the distance between the point 0 and B. The substitution of J_ω (A) by the specific intensity dJ_ω (Eq. (3.41)) leaving the unit of volume dV, gives

$$dJ_\omega^{(\alpha)}(\sigma) = \eta_\omega(\sigma)\, d\sigma \exp\left(-\int_\sigma^s \alpha_\omega\, d\sigma\right).$$

With no reflecting walls, the explicit expression for the power loss due to synchrotron radiation emitted in the volume element dV is obtained by integrating the specific intensity $dJ_\omega^{(\alpha)}$ per unit of solid angle $d\Omega_V$ over the frequencies ω and over the last magnetic plasma surface S

$$dP_{\text{em},\Omega_V}(\sigma) = \int_\omega d\omega \int_S dS \, \cos(\mathbf{k}, \mathbf{N})\, \eta_\omega(\sigma)\, d\sigma \, \exp\left(-\int_\sigma^s \alpha_\omega(\sigma')\, d\sigma'\right) \quad (3.42)$$

with $d\mathbf{S} = \mathbf{N}dS$, where $\mathbf{k}$ is the direction of the ray path within the solid angle $d\Omega_V$ crossing dV.

Note that for each unit of plasma surface $d\mathbf{S}$, we only consider the ray path with a direction $\mathbf{k}$ which crosses the volume element dV, i.e. the plasma volume participating to the investigated emission. A relation between $\mathbf{k}$, $\mathbf{N}$ and σ thus exists.

Similar magnetic surfaces with elliptical cross-section: In the particular case of a magnetic confinement plasma, we are interested in the radiation emitted between two consecutive magnetic surfaces. Here we consider that all the magnetic surfaces are similar to the outer surface (plasma surface), which has an elliptical cross-section with elongation κ, with a similarity ratio ρ (the normalized radius).

In this case, the volume element is not dV but that formed by the space between two magnetic surfaces:

$$dV_\rho = (\partial V/\partial\rho)\ d\rho.$$

Expressing the variable ρ as a function of σ ($\rho = f(\sigma)$), the corresponding unit of normalized radius $d\rho$ is given by the relation

$$d\sigma = Q(\rho, \Omega_\rho, S)\ d\rho,$$

and the synchrotron power loss in terms of the emission of such an element of volume characterized by ρ, is obtained by integrating Eq. (3.42) over the interval of solid angles Ω_ρ crossing the volume element dV_ρ,

$$dP_{\text{em}}(\rho) = \int_\omega d\omega \int_S dS \int_{\Omega_\rho} d\Omega_\rho \cos(\mathbf{k}, \mathbf{N}) \quad (3.43)$$

$$\times \sum_{j=1,2}\left[\eta_\omega(\sigma_j)\, Q(\rho, \Omega_\rho, S)\, d\rho \exp\left(-\int_{\sigma_j}^s \alpha_\omega^{(i)}(\sigma')\ d\sigma'\right)\right].$$

3. Study of synchrotron power losses in tokamak plasmas

Let us notice that for each ray path crossing dV_ρ, there are two intersection points $\sigma_j\left(\rho, \Omega_\rho, S\right)$ with $j = 1, 2$. To take into account the total emission of the volume element dV_ρ to $dP_{\text{em}}\left(\rho\right)$ we must add the contribution of both points.

According to Eq. (3.36) for the plasma surface and expressing the interval of solid angles in the exit point of the plasma as a function of the angle Θ between the direction of the ray path and the magnetic field, and the angle β between the projection of the ray path on the plane perpendicular to the magnetic field and the normal to the plasma surface, we obtain

$$\cos(\mathbf{k}, \mathbf{N}) = \sin\Theta\cos\beta,$$

$$dV_\rho = 4\pi^2 R a^2 \kappa \rho d\rho,$$

and

$$\int_{\Omega_\rho} d\Omega_\rho = 2\int_0^{\pi/2} \sin\Theta d\Theta \int_{\beta_{\min}}^{\beta_{\max}} d\beta,$$

with $\beta_{\min}$ and $\beta_{\max}$ the beta angle limits for which the ray path is tangent to the element of volume dV_ρ, so that

$$\beta_{\min}, \beta_{\max} = f\left(\rho, \Theta, \varphi\right).$$

Finally, the spatial density of the synchrotron power loss in terms of emission, denoted as dP_{em}/dV, is obtained by dividing Eq. (3.43) by the element of volume dV_ρ. For the two modes of propagation and using the normalized frequency $\nu = \omega/\omega_{ce}$, we obtain

$$\frac{dP_{\text{em}}\left(\rho\right)}{dV} = \frac{k}{4\pi^4 c^2}\frac{T_e\left(\rho\right)}{a\kappa}\int_0^\infty \nu^2 d\nu \int_0^\pi \left(\sin^2\varphi + \kappa^2\cos^2\varphi\right)^{1/2} d\varphi$$

$$\times \int_0^{\pi/2} \sin^2\Theta \, d\Theta \int_{\beta_{\min}}^{\beta_{\max}} \cos\beta \, d\beta \sum_{j=1,2} \left\{\omega_{ce,\text{loc}}^3\left(\sigma_j\right)\right.$$

$$\left.\times \sum_{i=o,x}\left[\alpha_\omega^{(i)}\left(\sigma_j\right)\frac{Q\left(\rho, \varphi, \Theta, \beta\right)}{\rho}\exp\left(-\int_{\sigma_j}^s \alpha_\omega^{(i)}\left(\sigma'\right)d\sigma'\right)\right]\right\}, \quad (3.44)$$

where $\omega_{ce,\text{loc}}$ is the electron cyclotron frequency at the point σ_j considered, and the temperature $T_e\left(\rho\right)$ is constant over the same magnetic surface ρ, i.e. $T_e\left(\rho\right) = T_e\left(\sigma_1\right) = T_e\left(\sigma_2\right)$.

This is the general formulation of the spatial density of the synchrotron power loss in terms of emission. Then, the functions Q, σ_j ,$\beta_{\min}$, and $\beta_{\max}$ are specific for each particular configuration: cylindrical geometry, toroidal geometry, circular cross-section ($\kappa = 1$), and elliptical cross-section ($\kappa > 1$).

The volume integral of the quantity dP_{em}/dV gives the global synchrotron power loss in the absence of wall reflections

$$P_{\text{syn}_0} = \int_0^1 \left(\frac{dP_{\text{em}}(\rho)}{dV} \right) \left(\frac{dV_\rho}{d\rho} \right) d\rho. \qquad (3.45)$$

3.7.2 Case of a plasma with cylindrical geometry

In the cylindrical case, the angle between the ray path direction and the magnetic field is constant along the ray path, so that $\theta = \Theta$.

Circular cross-section and homogeneous plasma: In a plasma with circular cross-section ($\kappa = 1$) and cylindrical geometry, there is a symmetry with respect to the poloidal angle φ. As shown in Fig. 3.12, for a given ray path direction with a β angle in the interval $[\beta_{\text{min}}, \beta_{\text{max}}]$, we obtain two points crossing the element of volume characterized by the magnetic surface ρ with the following ray path co-ordinates:

$$\sigma_{\perp 1,2} = a \left[\cos \beta \mp \left(\rho^2 - \sin^2 \beta \right)^{1/2} \right],$$

where $\sigma_{\perp i}$ is the perpendicular projection of the ray path,

$$\sigma_j = \frac{\sigma_{\perp j}}{\sin \theta}.$$

The ray path is tangent to the volume element dV_ρ when

$$\sin(\beta_{\text{max}}) = \rho,$$

and $\beta_{\text{min}} = -\beta_{\text{max}}$.

In this case, the $Q = d\sigma/d\rho$ factor due to the introduction of the ρ variable in the formalism becomes

$$Q(\rho, \theta, \beta) = \frac{a\rho}{\sin \theta \left(\rho^2 - \sin^2 \beta \right)^{1/2}}.$$

The explicit expression of the spatial density of the synchrotron power loss in terms of emission (Eq. (3.44)) for cylindrical and homogeneous plasmas with circular cross-section (so that $\kappa = 1$), can be then written as

$$\frac{dP_{\text{em}}(\rho)}{dV} = \frac{k}{4\pi^3 c^2} \omega_{ce}^3 T_e \int_0^\infty \nu^2 d\nu \int_{\beta_{\text{min}}}^{\beta_{\text{max}}} \frac{\cos \beta}{\left(\rho^2 - \sin^2 \beta \right)^{1/2}} d\beta$$

$$\times \int_0^{\pi/2} \sin \theta \, d\theta \sum_{j=1,2} \left\{ \sum_{i=o,x} \left[\alpha_\omega^{(i)} \exp \left(-\alpha_\omega^{(i)} \sigma_j \right) \right] \right\} \qquad (3.46)$$

with $T_e(\rho) = T_e$, $\omega_{ce,\text{loc}} = \omega_{ce}$ and $\alpha_\omega^{(i)}(\sigma_j) = \alpha_\omega^{(i)}$.
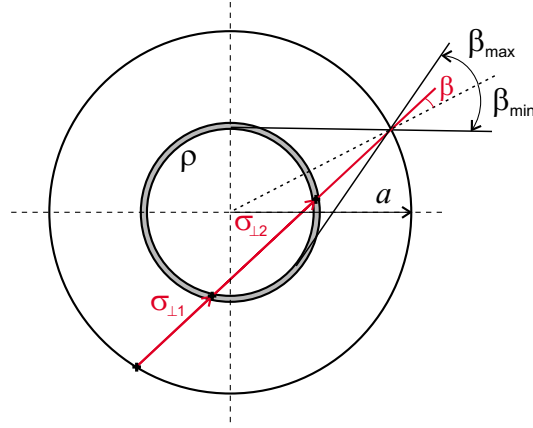
Figure 3.12: Geometry of the ray path and ρ magnetic surface intersection in the perpendicular plane to the cylindrical plasma.

Elliptical cross-section and inhomogeneous plasma: Let us consider now an elliptical cross-section plasma with elongation κ. In this case, the intersection of the ray path with the ρ magnetic surface depends on the poloidal angle φ. The β angles for each magnetic surface obey to the following implicit condition $\beta_{\min} < \beta < \beta_{\max}$, with:

$$\frac{(1-\rho^2)}{(\sin^2\varphi + \kappa^2\cos^2\varphi)^2} \leq \kappa^2\sin^2\beta\cos^2\beta - 2\kappa(\kappa^2-1)\sin\varphi\cos\varphi\sin\beta\cos^3\beta$$
$$+ (\sin^2\varphi + \kappa^4\cos^2\varphi)\cos^4\beta,$$

taking into account that

$$\beta_{\min} < \beta_0 \quad \text{and} \quad \beta_{\max} > \beta_0,$$

where $\beta_0(\kappa,\varphi)$ is the β angle made by the ray path when crossing the plasma centre. It is found that

$$\cos\beta_0 = \frac{\kappa}{(\cos^2\varphi + \kappa^2\sin^2\varphi)^2(\sin^2\varphi + \kappa^2\cos^2\varphi)^2}.$$

The ray path co-ordinates for the intersection points with the element of volume characterized by the magnetic surface ρ, result in

$$\sigma_{1,2} = \frac{as^\star\cos\beta}{\sin\theta}\left[1 \mp \sqrt{1 - \frac{(1-\rho^2)}{S}}\right],$$

where $s^\star(\kappa,\varphi,\beta)$ and $S(\kappa,\varphi,\beta)$ are defined in Eqs (3.37) and (3.40), respectively. Introducing the variable $u = \frac{\sin\theta}{as^\star\cos\beta}\sigma$, we obtain

$$u_{1,2} = 1 \pm \sqrt{1 - \frac{(1-\rho^2)}{S}}.$$

In the elliptical case, the $Q_u = du/d\rho$ factor due to the introduction of the ρ variable in the formalism becomes

$$Q_u\left(\kappa, \varphi, \beta\right) = \frac{\rho}{S\sqrt{1 - \frac{(1-\rho^2)}{S}}},$$

and Eq. (3.44) can be written as

$$\frac{dP_{\text{em}}\left(\rho\right)}{dV} = \frac{k}{4\pi^4 c^2} T_e\left(\rho\right) \int_0^\infty \nu^2 d\nu \int_0^\pi d\varphi \int_0^{\pi/2} d\theta \int_{\beta_{\min}}^{\beta_{\max}} d\beta \frac{\sin\theta}{\sqrt{1 - \frac{(1-\rho^2)}{S}}}$$

$$\sum_{j=1,2} \left\{ \omega_{ce}^3\left(u_j\right) \sum_{i=o,x} \left[\alpha_\omega^{(i)}\left(u_j\right) \exp\left(-\frac{as^\star \cos\beta}{\sin\theta} \int_{u_j}^2 \alpha_\omega^{(i)}\left(u'\right) \, du'\right) \right] \right\},$$

$$\tag{3.47}$$

In Eq.3.47, the optical depth for each ray path co-ordinate u' is calculated using the local values of plasma parameters, i.e. local density $n_e\left(\rho'\right)$ and temperature $T_e\left(\rho'\right)$, where the local normalized radius ρ' is calculated using Eq. (3.39). The magnetic field $B_t\left(r_h\right)$ is given by

$$B_t\left(r_h\right) = \frac{B_{t_0}}{1 + r_h/R}, \tag{3.48}$$

where B_{t_0} is the magnetic field at the magnetic axis and r_h is the horizontal co-ordinate on the corresponding poloidal cross-section, whose origin is placed at the centre of such a cross-section,

$$r_h = a \left[\cos\varphi + \left(2 - u'\right) s^* \cos\beta \frac{\left(\sin\beta \sin\varphi - \kappa \cos\beta \cos\varphi\right)}{\left(\sin^2\varphi + \kappa^2 \cos^2\varphi\right)^{1/2}} \right].$$

The local electron cyclotron frequency is expressed as $\omega_{ce}\left(u\right) = e/m_e B_t\left(r_h\right)$.

Fig. 3.13 shows the dP_{em}/dV profile for the European Commercial Reactor [Coo99] taking flat profiles for the density and temperature and considering the operating point $n_e = 0.85 \times 10^{20}$ m^{-3} and $T_e = 22.7$ keV. If the magnetic field is also kept constant in all the plasma volume, the spatial density of radiation emission is homogeneous whereas the plasma self-absorption of the emitted radiation is much lower in the more external plasma layers. For this reason, the spatial density of synchrotron power losses in terms of emission is strongly peaked in those external layers. The same behaviour is observed when we add the inhomogeneity of the magnetic field, which makes the emission to increase softly in the outer plasma.

With no wall reflections, the global synchrotron losses corresponding to the homogeneous and inhomogeneous magnetic field are $P_{\text{syn}_0} \simeq 202$ MW and $P_{\text{syn}_0} \simeq 248$ MW, respectively.
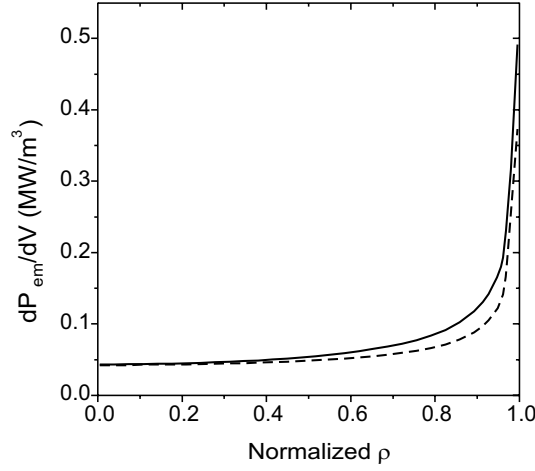
Figure 3.13: Spatial density of synchrotron power losses in terms of emission considering flat density and temperature profiles with a homogeneous magnetic field (dashed curve), and with an inhomogeneous magnetic field (solid curve).

3.8 Radiation transport in a toroidal geometry

3.8.1 Explicit expression for the calculation of synchrotron power loss

Using the co-ordinates and angles defined in Fig. 3.14, one can write the equation describing the torus surface in the absolute frame xyz as

$$\left(x^2 + y^2 + \frac{z^2}{\kappa^2} + R^2 - a^2 \right)^2 - 4R^2 \left(x^2 + y^2 \right) = 0.$$

Notice that the angles Ψ, Θ, φ , and β are defined at the point of the ray path emerging from the plasma. Then, the origin of the ray path is located on the opposite side, i.e. at the entry point of the plasma. The parametric equation of the ray path line in the same system can be written as

$$\begin{cases} x = p_x + (s - \sigma)\,\gamma_x \\ y = p_y + (s - \sigma)\,\gamma_y \\ z = p_z + (s - \sigma)\,\gamma_z, \end{cases} \qquad (3.49)$$

where p_x, p_y, and p_z are the co-ordinates of the origin of the relative frame $x'y'z'$, i.e. the intersection of the ray path with the torus surface in the exit point $(\sigma = s)$,
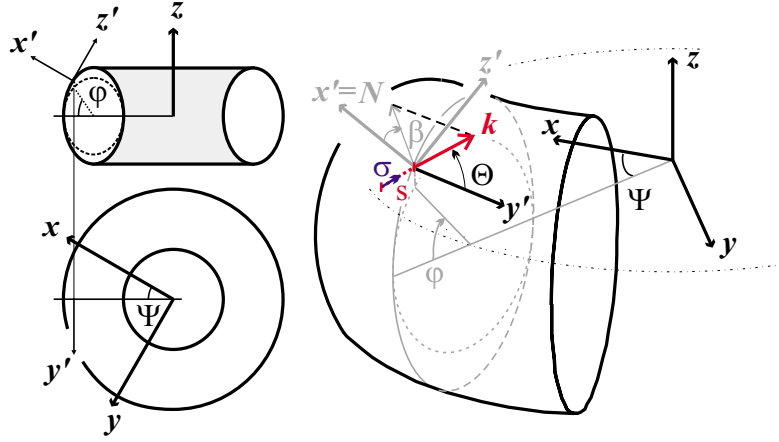
Figure 3.14: Angle and axis definitions for a toroidal plasma geometry.

which can be expressed in the absolute frame as

$$
\begin{cases}
p_x = (R + a\cos\varphi)\cos\Psi \\
p_y = (R + a\cos\varphi)\sin\Psi \\
p_z = a\kappa\sin\varphi.
\end{cases}
\tag{3.50}
$$

Here, $(\gamma_x,\, \gamma_y,\, \gamma_z)$ is the unit vector of the ray path trajectory expressed in the absolute frame, namely

$$
\begin{cases}
\gamma_x = -\gamma'_y\sin\Psi + \dfrac{\gamma'_x\,\kappa\cos\varphi - \gamma'_z\sin\varphi}{(\sin^2\varphi + \kappa^2\cos^2\varphi)^{1/2}}\cos\Psi \\[2mm]
\gamma_y = \gamma'_y\cos\Psi + \dfrac{\gamma'_x\,\kappa\cos\varphi - \gamma'_z\sin\varphi}{(\sin^2\varphi + \kappa^2\cos^2\varphi)^{1/2}}\sin\Psi \\[2mm]
\gamma_z = \dfrac{\gamma'_x\sin\varphi + \gamma'_z\,\kappa\cos\varphi}{(\sin^2\varphi + \kappa^2\cos^2\varphi)^{1/2}},
\end{cases}
\tag{3.51}
$$

where $\left(\gamma'_x, \gamma'_y, \gamma'_z\right)$ is the same vector expressed in the relative frame as

$$
\begin{cases}
\gamma'_x = -\sin\Theta\cos\beta \\
\gamma'_y = -\cos\Theta \\
\gamma'_z = -\sin\Theta\sin\beta.
\end{cases}
$$

Considering the axisymmetric geometry, we take $\Psi = 0$, and Eqs (3.50) and (3.51) let

$$
\begin{cases}
p_x = R + a\cos\varphi \\
p_y = 0 \\
p_z = a\kappa\sin\varphi
\end{cases}
\tag{3.52}
$$

76

$$\begin{cases} \gamma_x = \dfrac{\gamma'_x \, \kappa \cos\varphi - \gamma'_z \sin\varphi}{(\sin^2\varphi + \kappa^2 \cos^2\varphi)^{1/2}} \\[2ex] \gamma_y = \gamma'_y \\[2ex] \gamma_z = \dfrac{\gamma'_x \sin\varphi + \gamma'_z \, \kappa \cos\varphi}{(\sin^2\varphi + \kappa^2 \cos^2\varphi)^{1/2}}. \end{cases} \qquad (3.53)$$

We can then derive the length s of the ray path, given by the intersection of the torus surface with the ray at the entry point. Thus, imposing $\sigma = 0$ in Eqs (3.49), we obtain the following cubic equation for the calculation of s:

$$As^3 + Bs^2 + Cs + D = 0, \qquad (3.54)$$

with

$$A = \left(\gamma_x^2 + \gamma_y^2 + \frac{\gamma_z^2}{\kappa^2} \right)^2$$

$$B = 4 \left(\gamma_x^2 + \gamma_y^2 + \frac{\gamma_z^2}{\kappa^2} \right) \left(p_x \gamma_x + \frac{p_z \gamma_z}{\kappa^2} \right)$$

$$C = 4 \left(p_x \gamma_x + \frac{p_z \gamma_z}{\kappa^2} \right)^2 + 2 \left(\gamma_x^2 + \gamma_y^2 + \frac{\gamma_z^2}{\kappa^2} \right)$$
$$\times \left(p_x^2 + \frac{p_z^2}{\kappa^2} + R^2 - a^2 \right) - 4R^2 \left(\gamma_x^2 + \gamma_y^2 \right)$$

$$D = 4 \left(p_x \gamma_x + \frac{p_z \gamma_z}{\kappa^2} \right) \left(p_x^2 + \frac{p_z^2}{\kappa^2} + R^2 - a^2 \right) - 8R^2 p_x \gamma_x.$$

The resolution of the above equation may lead to one of the following three cases, whose geometrical meaning is illustrated in Fig. 3.15.

Case a: One positive real solution (A) and two imaginary solutions (B and C). The ray path crosses the torus surface only once (A).

Case b: Three positive real solutions. The ray path crosses the torus two more times (B and C) but in a different plasma section.

Case c: One positive real solution (A) and two negative real solutions (B and C). The negative solutions are not taken into account since the ray emerging from the torus does not enter back at a different point (B).

Hence, the length of the ray path s is always the smallest real positive solution.

Let us now define the horizontal co-ordinate r_h, which appears in the calculation of the radial variation of the magnetic field (Eq. (3.48)). For every point σ of the
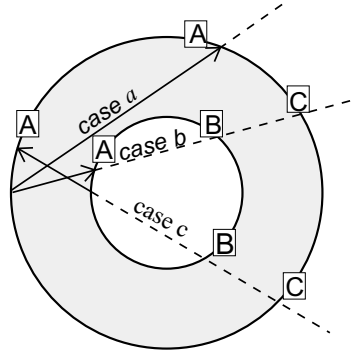
Figure 3.15: Geometrical interpretation of the three solutions of Eq. (3.54) in the case of a horizontal ray path.

ray path, the horizontal co-ordinate r_h on the corresponding poloidal cross-section, whose origin is placed at the centre of such a cross-section, becomes

$$r_h = \sqrt{x^2 + y^2} - R, \tag{3.55}$$

where $x(\sigma)$ and $y(\sigma)$ are the horizontal co-ordinates of the parametric equations of the ray path line.

With the above equations, the calculation of the normalized radius ρ as a function of the co-ordinate along the ray path σ can be expressed as

$$\rho^2 = \frac{1}{a^2} \left[r_h^2 + \left(\frac{z}{\kappa} \right)^2 \right], \tag{3.56}$$

where $z(\rho)$ is the vertical co-ordinate of the parametric equation of the ray path.

In toroidal plasmas, the parallel refraction index $N_{\parallel}$ varies along the ray path because the angle θ between the direction of the ray path and the magnetic field is a function of space. Such a variation must be taken into account in the calculation of the plasma self-absorption.

The direction of the ray path is fully determined in the absolute frame by the unit vector $\mathbf{u} = (\gamma_x, \gamma_y, \gamma_z)$. In the same frame, the unit vector $\mathbf{b} = \mathbf{B}/B$ at the point determined by the space co-ordinate σ along the ray path can be expressed as

$$\mathbf{b} = \frac{(-\tan \Psi, 1, 0)}{\sqrt{1 + \tan^2 \Psi}},$$

where

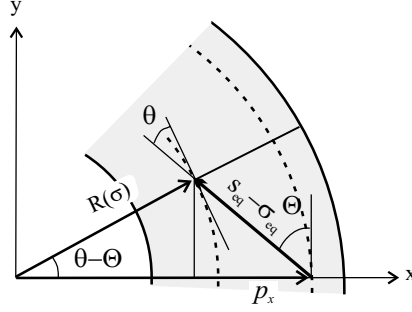$$\tan \Psi = \frac{(s - \sigma) \, \gamma_y}{p_x + (s - \sigma) \, \gamma_x}.$$

Figure 3.16: $N_\parallel$ variation along the ray path in the equatorial plane, where s_{eq} and σ_{eq} are the projections of the ray path length and ray path co-ordinate, respectively, on the equatorial plane.

Now, since $\cos\theta = \mathbf{u} \cdot \mathbf{b}$, we can derive the following simple relation between the angles θ and Θ for a given ray path and co-ordinate σ

$$\cos\theta = \cos\Theta \frac{p_x}{R(\sigma)}, \tag{3.57}$$

where p_x is defined in Eq. (3.52) and

$$R(\sigma) = \sqrt{x^2 + y^2} \tag{3.58}$$

is the horizontal co-ordinate in the equatorial plane, whose origin is placed at the tokamak centre. Fig. 3.16 shows the equatorial projections of the ray path on the tokamak plasma. Only positive values of $\cos\theta$ may be considered, as it can be shown that $\alpha_\omega^{(i)}(\pi - \theta) = \alpha_\omega^{(i)}(\theta)$.

In such a realistic plasma conditions with no reflecting walls, toroidal geometry, and an elliptical cross-section with a vertical elongation κ (Fig. 3.14), Eqs (3.22) and (3.12) including the ordinary (o) and extraordinary (x) modes of propagation become

$$\Phi^* = \frac{3R^3}{2\pi^3 p_{a_0}} \int_0^\infty \nu^2 d\nu \int_0^\pi (\sin^2\varphi + \kappa^2 \cos^2\varphi)^{1/2} d\varphi \int_0^{\pi/2} \sin^2\Theta \, d\Theta$$

$$\times \int_{-\pi/2}^{\pi/2} \cos\beta \, d\beta \int_0^s \frac{F_T(\rho)}{R^3(\sigma)} \sum_{i=o,x} \left\{ \alpha_\omega^{(i)}(\sigma) \exp\left[-\int_\sigma^s \alpha_\omega^{(i)}(\sigma') \, d\sigma' \right] \right\} d\sigma$$

$$\tag{3.59}$$

with an arbitrary temperature profile expressed as

$$T_e(\rho) = T_{e_0} \, F_T(\rho),$$

p_{a_0} is defined using Eq. (3.28) with values at the plasma axis, and where the frequency ω is normalized to the electron cyclotron frequency $\omega_{ce}(\sigma)$ corresponding to the ray path co-ordinate σ, so then $\nu = \omega/\omega_{ce}(\sigma)$. For a given σ (and $\omega_{ce}(\sigma)$) the electron cyclotron frequency corresponding to the co-ordinate σ' of the optical depth calculation may be higher or lower than $\omega_{ce}(\sigma)$, as discussed in Section 3.8.1. It can be seen that

$$\frac{\omega_{ce}(\sigma)}{\omega_{ce_0}} = \frac{R}{R(\sigma)}.$$

According to the definition of the dimensionless parameter Φ^* and using Eq. (3.21) with values at the plasma axis, synchrotron power losses become

$$P_{\text{syn}_0} = \frac{2\pi k}{3c^3} \omega_{pe_0}^2 \omega_{ce_0}^2 a^2 R T_{e_0} \Phi^*, \tag{3.60}$$

where ω_{ce_0} and ω_{pe_0} are the electron cyclotron and plasma frequencies at the magnetic axis. The description of the plasma emission and self-absorption processes includes the above described phenomena of inhomogeneity of the magnetic field, toroidal correction to the ray path length and the spatial variation of $N_\parallel$.

For a practical computation of Eq. (3.59), the interval for the normalized frequency is taken to be $\nu = [2, 40]$. Let us notice that $\nu = 2$ is the minimum value allowed by the quasi-exact method for the calculation of the absorption coefficient [Gra91]. In the range of parameters of interest for the synchrotron losses problem, radiation emitted below the lower ν limit or above the upper ν limit is negligible with respect to the emission within the ν interval.

Treatment of low frequency waves: As a consequence of the inhomogeneity of the magnetic field in a poloidal section, the electron cyclotron frequency is no longer constant along a ray path. Low frequency waves propagating towards the plasma region with high magnetic field can then reach the cut-off frequency, which we normalize to the electron cyclotron frequency ($\nu_{\text{cut-off}}$). In such a situation, occurring mainly in very low aspect ratio plasmas ($A < 2$), we assume the waves to be reflected and finally absorbed by the plasma.

For a given tokamak plasma (R, a, κ) and ray path (φ, Θ, β), the point reaching the highest magnetic field (so that the highest electron cyclotron frequency $\omega_{ce}(\sigma)$) is that with a minimum horizontal co-ordinate r_h, as seen in the equatorial projection of Fig. 3.17. Assuming a constant cut-off frequency along the ray path, this is the most critical point where the local normalized frequency of the ray path $\nu = \omega_{ce}(\sigma)$ is minimum and the cut-off may then occur ($\nu < \nu_{\text{cut-off}}$).

As a first estimation, let us consider the cut-off frequency in the cold plasma approximation:

$$\nu_{\text{cut-off}} = \frac{1}{2} \left(1 + \sqrt{1 + 4\omega_{pe}^2/\omega_{ce}^2} \right). \tag{3.61}$$
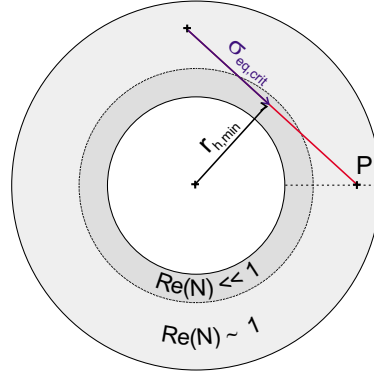
80

Figure 3.17: Ray path trajectory on the equatorial plane of the tokamak in the case of a low frequency wave propagating towards the high magnetic field region.

For the plasmas of interest we have $\omega_{ce} > \omega_{pe}$, and then for the above conditions we obtain $\nu_{\text{cut-off}} < 1.62$ (lower than the low frequency integration limit).

For the determination of the critical point σ_{crit} through the ray path trajectory, we perform the ν minimisation (i.e. the r_h minimisation) as $\frac{d}{d\sigma}(r_h) = 0$, leading to

$$\sigma_{\text{crit}} = s + p_x \frac{\gamma_x}{\gamma_x^2 + \gamma_y^2}.$$

Note that if the minimum exists within the ray path trajectory, σ_{crit} must fulfil the condition $0 < \sigma_{\text{crit}} < s$. Therefore, when the unit vector of the ray path points to the inner plasma (region with higher magnetic field), i.e. $\gamma_x > 0$, the critical point is always situated at the exit point of the plasma, $\sigma_{\text{crit}} = s$. On the contrary, when the unit vector of the ray path points to the outer plasma (region with lower magnetic field), i.e. $\gamma_x < 0$, a minimum of ν may occur at an intermediate point, as illustrated in Fig. 3.17.

In both cases, the minimum normalized frequency $\nu_{\min}$ at the critical point σ_{crit} can be calculated as a function of the initial co-ordinate and frequency (σ and ν) and if $\nu_{\min}$ is lower than the cut-off normalized frequency, we assume the wave to be totally absorbed by the plasma. In such a case, we will perform the integration of the radiative transfer equation (Eq. (3.10)) over the ray path interval $[s_{\min}, s]$, where $s_{\min}(\nu)$ is the minimum ray path co-ordinate at a given normalized frequency for which the wave does not reach the cut-off normalized frequency. It can be seen that

$$s_{\min} = s + \frac{p_x \gamma_x - \sqrt{\left(\gamma_x^2 + \gamma_y^2\right) R_{\text{crit}}^2 \left(\nu/\nu_{\text{cut-off}}\right)^2 - p_x^2 \gamma_y^2}}{\left(\gamma_x^2 + \gamma_y^2\right)}$$

with $R_{\text{crit}} = \sqrt{\left(p_x + (s - \sigma_{\text{crit}})\gamma_x\right)^2 + (s - \sigma_{\text{crit}})^2 \gamma_x^2}$. In this case, the useful ex-

pression for the calculation of synchrotron losses is written as

$$\Phi^* = \frac{3R^3}{2\pi^3 p_{a_0}} \int_0^\infty \nu^2 d\nu \int_0^\pi (\sin^2 \varphi + \kappa^2 \cos^2 \varphi)^{1/2} d\varphi \int_0^{\pi/2} \sin^2 \Theta \, d\Theta$$

$$\times \int_{-\pi/2}^{\pi/2} \cos \beta \, d\beta \int_{s_{\min}}^s \frac{F_T(\rho)}{R^3(\sigma)} \sum_{i=o,x} \left\{ \alpha_\omega^{(i)}(\sigma) \exp\left[- \int_\sigma^s \alpha_\omega^{(i)}(\sigma') \, d\sigma' \right] \right\} d\sigma.$$

In spite of this assumption in the treatement of low frequency waves and for plasma parameters of interest, the total synchrotron losses in this case are not substantially different from the other extreme case, where the waves reaching $\nu_{\text{cut-off}}$ are neither reflected nor absorbed by the plasma. The reason for this lack of sensitivity is that plasmas with appreciable total synchrotron losses (the interesting case) emit mainly in the frequency range above three or four times the electron cyclotron frequency.

3.8.2   Aspect ratio effect

In Figs. 3.18 and 3.19, we illustrate the aspect ratio ($A = R/a$) dependence for a plasma with toroidal geometry choosing the nominal parameters of the European Commercial Reactor[4] [Coo99]: $R = 8.1$ m, $a = 2.7$ m, $B_{t_0} = 6.8$ T. For the aspect ratio variation, we assume a constant plasma volume.

In the first plot (Fig. 3.18), we consider a plasma with a circular cross-section ($\kappa = 1$) and flat density and temperature profiles. In such conditions, the results can be compared with those of Trubnikov's fit [Tru79] including the correction factor due to the inhomogeneity of the magnetic field (see Section 3.4). In the second one (Fig. 3.19), we consider an elliptical plasma with the nominal elongation $\kappa = 1.9$, and generalized parabolic profiles for density and temperature with the nominal peaking parameters $\alpha_n = 0.5$ and $\alpha_T = 1.0$ in Eq. (3.25). Here, complete calculations in toroidal or cylindrical plasmas are compared with the FMGG fit [Fid92], which keeps the same dependences on temperature, density, magnetic field, and major and minor radii as Trubnikov's fit, as well as the approximate correction due to the toroidal inhomogeneity of the magnetic field.

Synchrotron losses in both illustrations increase with increasing aspect ratio since the plasma becomes increasingly thinner, causing the optical depth of the emitted radiation in the plasma centre to decrease. As a confirmation, the numerical calculation for high aspect ratios in toroidal geometry tends towards the one of the cylindrical approach. As the aspect ratio decreases, the magnetic field strongly increases in the inner part of the plasma cross-section, resulting in the growth of synchrotron losses despite a slight attenuation due to the toroidal correction to the ray path length.

---

[4]Note that the synchrotron losses do not take wall reflections into account.
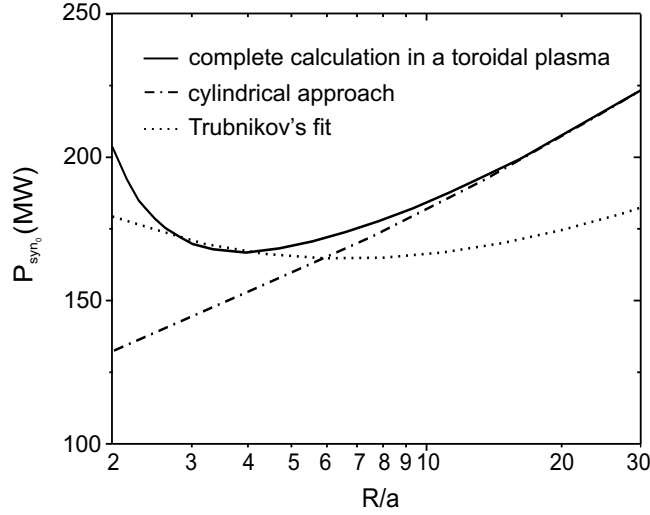
Figure 3.18: Comparison of the complete calculation of synchrotron losses in a toroidal or cylindrical plasma geometry with the results of Trubnikov's fit, for a circular cross-section and flat density and temperature profiles ($T_e = 30\,\text{keV}$).

We can see that the numerical results from the complete formulation agree well with the Trubnikov and FMGG fits, for intermediate aspect ratios in the range $2.5 < A < 4.5$ (for Trubnikov's fit) and in the range $3.2 < A < 4.2$ (for the FMGG fit). Note that effects of the toroidal correction to the ray path length and of the spatial variation of $N_\parallel$ are not included in the Trubnikov and FMGG fits. The explanation of the observed agreement is that the errors introduced with the description simplified phenomena and geometry, and by the approximations in the absorption calculation, are self-compensating for this aspect ratio interval. However, the results differ substantially for larger or smaller aspect ratios, which can be of interest for a commercial reactor.

3.8.3 Effect of temperature profiles

Generalized parabolic profiles: The effect of the shape of temperature profiles is illustrated by comparing synchrotron power losses for the European Commercial Reactor parameters [Coo99] with a constant density profile and density averaged electron temperature $\langle T_e \rangle_n$,

$$\langle T_e \rangle_n = \frac{\int_V n_e T_e dV}{\int_V n_e dV}.$$

In other words, we compare different shapes of temperature profiles but keeping the same plasma energy content W_{th}. Nominal parameters give $\langle T_e \rangle_n \simeq 27.2$ keV
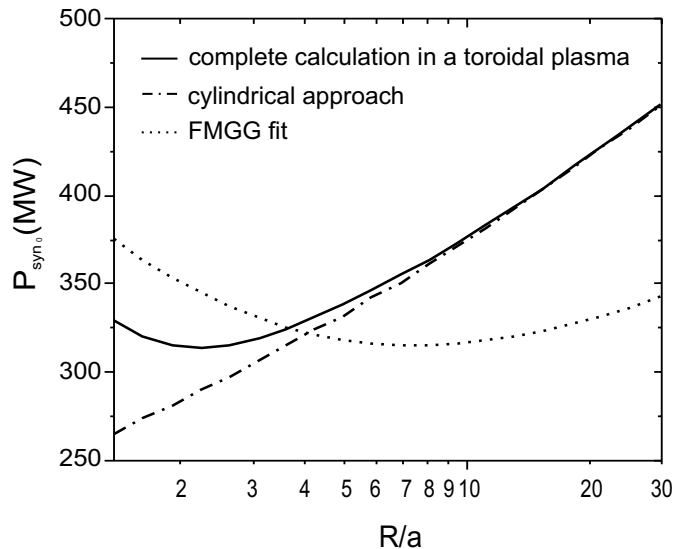
Figure 3.19: Comparison of the complete calculation of synchrotron losses in a toroidal or cylindrical plasma geometry with the results of the FMGG fit, for a large interval of aspect ratios ($\langle T_e \rangle = 22.7\,\text{keV}$).

and $W_{\text{th}} \simeq 2190$ MJ. We consider generalized parabolic expressions (Eq. (3.25)) for modelling profiles of density and temperature with $n_{e_0} = 1.5 \times 10^{20}$ m^{-3}, $\alpha_n = 0.5$.

Fig. 3.20 shows the shape of such profiles for $\alpha_T = 0$, 0.5, 1.0, 1.5, 2.0 (a), and the corresponding synchrotron losses calculated without wall reflections in toroidal realistic conditions (b), using Eqs (3.59) and (3.60). Although the plasma energy content is kept constant for any value of α_T, we observe a substantial rise of synchrotron power losses from $\alpha_T = 0.5$ to $\alpha_T = 2.0$. In the latter point, they are about twice those of a flat ($\alpha_T = 0$) or slightly peaked ($\alpha_T = 0.5$) profiles.

The strong effect of the temperature profile shape on synchrotron losses can be explained using the spatial density of the synchrotron power loss in terms of emission dP_{em}/dV (Fig. 3.20 (a)). In contrast to the homogeneous case (Fig. 3.13), for $\alpha_T > 0$ the plasma layers participating the most to the global synchrotron loss are not external but central. In consequence, the most sensitive parameters to the global synchrotron loss are the temperature and density on the plasma axis. The second observation taken out from these curves is the strong increase of dP_{em}/dV with the value of the electron temperature.

The effect of the shape of temperature profiles described by generalized parabolic expressions (Eq. (3.25)), has been shown in Ref. [Tam88]. This effect has also been included in the FMGG fit [Fid92]. Note that differences between our calculations
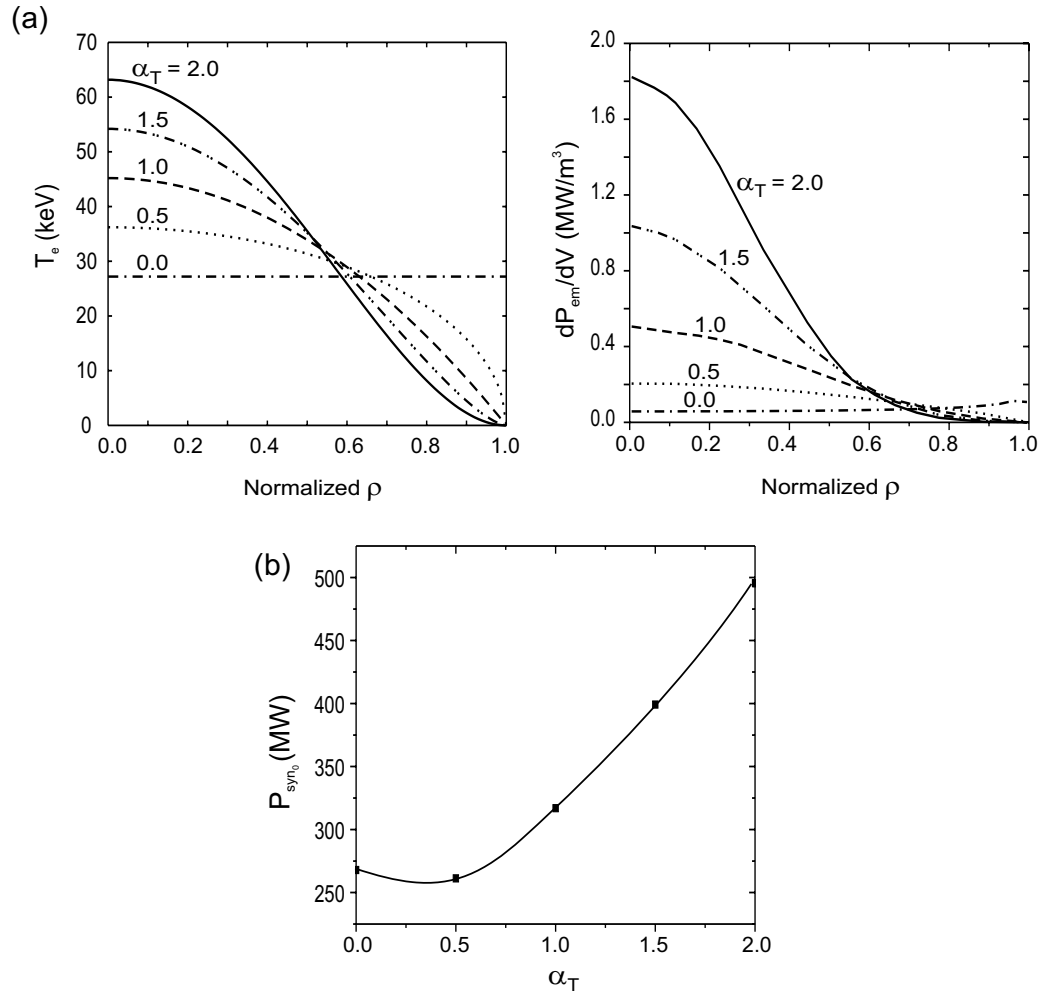
Figure 3.20: (a) On the left side, electron temperature profiles described by generalized parabolic expressions with $\alpha_T = 0, 0.5, 1.0, 1.5, 2.0$, keeping the density averaged temperature constant; on the right side, the corresponding power loss spatial density in terms of emission; (b) evolution of synchrotron losses with the peaking parameter α_T.

and those of FMGG fit are lower than 9% for the above profiles.

"Advanced" profiles: Next, we will see that temperature profiles in internal transport barrier (ITB) regimes, which are of considerable interest for a reactor, cannot be described accurately with such expressions, as far as synchrotron losses are concerned.

In order to quantify the effect of arbitrary profiles for the electron temperature on the global synchrotron losses, we compare the results considering two different models for the electron temperature profile. The first one is a simple model for an "advanced" temperature profile typical of ITB regimes, which is characterized by the ITB position ρ_{ITB} expressed in normalized radius (see Fig. 3.21). The temperature at the magnetic axis is taken to be 40 keV, and the temperature at the plasma edge is taken to be 1 keV. In this model, the slopes inside the ITB and in the outer part of the plasma cross-section are fixed to $4.17 T_0$ and $0.45 T_0$, respectively, as well as the temperature at the inside boundary of the ITB ($0.9 T_0$) and the edge temperature ($T_{\text{edge}} = 1$ keV).

The second model for the electron temperature profile is a generalized parabolic model, with the peaking parameter α_T giving the best fit[5] to the "advanced" model for the same value of the temperature at the magnetic axis (40 keV). The volume average temperatures and the energy content obtained with one or the other model are not significantly different.

We take the European Reactor nominal parameters with a fixed density profile given by a generalized parabolic profile ($n_{e_0} = 1.5 \times 10^{20}$ m^{-3}, $\alpha_n = 0.5$). In Fig. 3.21 we can see the substantial difference, around 20-40%, between global synchrotron losses computed with the "advanced" model and the generalized parabolic one. The absolute value of the power loss decreases for more central barrier positions owing to a lower plasma thermal energy content. On the other hand, the relative difference between the two temperature models increases when the ITB position is more central.

In Fig. 3.21 we see that dP_{em}/dV is peaked at the plasma centre in the case of an electron temperature profile described by a generalized parabolic model, whereas the maximum of dP_{em}/dV is displaced to the inside boundary of the ITB in the case of the "advanced" model. The emission and absorption processes, depending on the electron temperature, are competing to build the dP_{em}/dV profile: the radiation emission strongly increases with temperature, which is higher in the plasma centre, whereas the plasma self-absorption of the emitted radiation is lower in the more external plasma layers. In ITB confinement regimes, however, both conditions are met since the temperature is maintained at high values up to a non-central plasma layer; that is the reason why, for a same plasma thermal energy content, the synchrotron

---

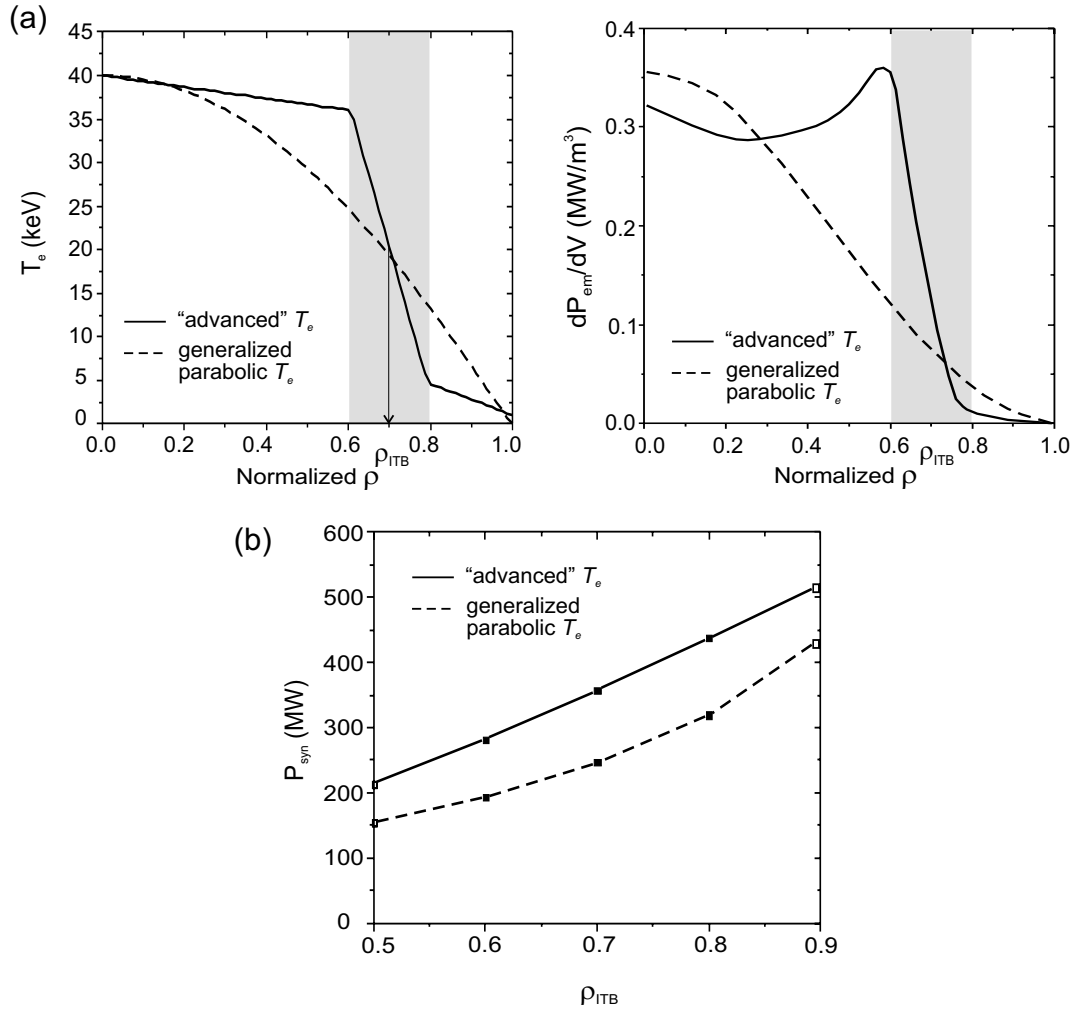[5]In the volume averaged least square meaning.

Figure 3.21: (a) On the left side, the electron temperature profile given by the "advanced" model with an ITB at 0.7 normalized radius, and the best fit generalized parabolic profile ($\alpha_T \simeq 1.1$); on the right side, the corresponding power loss spatial density in terms of emission; (b) synchrotron losses for different positions of the ITB for each temperature model.

losses are higher in such a regime. As a result, the power loss due to synchrotron radiation plays a more important role in the plasma power balance when the electron temperature has an "advanced" profile.

3.8.4 New fit for the calculation of global synchrotron losses

In the previous Sections we have shown that present approximate expressions (in particular the FMGG fit) do not describe correctly either the dependence of synchrotron losses on the aspect ratio or the important effect of temperature profiles with a shape different from a generalized parabolic one. On the other hand, the time required for the complete calculation of synchrotron losses with present day computers is unreasonable for system studies (typically 30 minutes CPU to obtain one value of Φ^* with a 2% precision using an Alpha EV6-500 processor). Therefore, a new fit for a fast calculation of the global synchrotron losses is derived using multiple non-linear regression, from a database consisting of about 3000 complete computations of Eq. (3.59).

In order to minimize the execution time required to build the database, the code (implementing the complete formulation) has been adapted and optimized for massively parallel processing. Computations have been performed on the parallel machine Compaq SC232, owning to the *Commissariat à l'Énergie Atomique*. Using 32 processors (type EV67-667) of such a machine, the calculation time to obtain one value of Φ^* has been reduced to typically two minutes CPU with a 2% precision.

Fitting variables: The dimensionless parameter p_{a_0} defined using Eq. (3.28) with values at the plasma axis, and in which the magnetic field and central density dependences are gathered, is used as a fitting variable. Strictly speaking, this combination appears only in the frame of Trubnikov's approximate method for the calculation of the absorption coefficients. Nevertheless, when the quasi-exact method is used, the synchrotron losses computed using different sets of magnetic field and central density resulting in the same central p_{a_0} parameter, differ by less than 5%.

The electron temperature profile is modelled using the following radial dependence:

$$T_e(\rho) = (T_{e_0} - T_{e_a}) \left(1 - \rho^{\beta_T}\right)^{\alpha_T} + T_{e_a}, \tag{3.62}$$

where α_T and β_T are peaking parameters for the electron temperature profile, and T_{e_a} is the edge electron temperature. Eq. (3.62) allows the description of a large variety of profiles including "advanced" profiles. Here, the edge electron temperature T_{e_a} is fixed to 1 keV for our calculations.

The density profile, on the other hand, is described using a generalized parabolic profile with peaking parameter α_n, since the maximum difference between synchrotron losses computed using an arbitrary density profile or using the correspond-
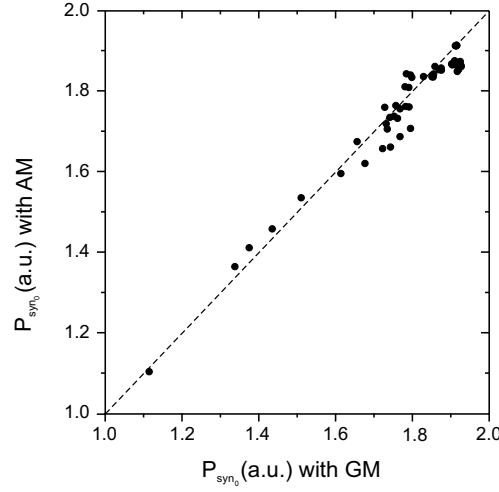
Figure 3.22: Synchrotron radiation losses computed with an "advanced" model (AM) for the density profile against those computed with the best generalized parabolic model (GM).

ing best generalized parabolic one, is always marginal. As an illustration, we compare the results considering an "advanced" model for the density profile (as that of Eq. (3.62)), with those considering the best parabolic profile which fits the "advanced" profile[6]. Fig. 3.22 shows the good agreement in the 58 pairs of numerical calculations of synchrotron losses using the first profile ($\alpha_n = [0, 8]$ and $\beta_n = [1, 8]$) or the latter one, with a maximum difference lower than 5%.

The other fitting variables are the temperature T_{e_0} at the magnetic axis and the plasma vertical elongation κ.

Regression result: After an exhaustive statistical analysis of interdependences between fitting variables, we propose the following fit for the global calculation of synchrotron losses, for an aspect ratio $A = 3$:

$$\Phi^*_{\text{fit } (A=3)} = 6.86 \times 10^{-5} \kappa^{0.79} \left(16 + T_{e_0}\right)^{2.61}$$
$$\times \left(p_{a_0}^{0.41} + 0.12\, T_{e_0}\right)^{-1.51} K\left(\alpha_n, \alpha_T, \beta_T\right), \qquad (3.63)$$

---

[6]In the volume averaged least square meaning, and for a given density at the plasma axis.

where T_{e_0} is expressed in keV and the profile factor K is given by the following expression:

$$
\begin{aligned}
K\left(\alpha_n, \alpha_T, \beta_T\right) = {} & \left(\alpha_n + 3.87\,\alpha_T + 1.46\right)^{-0.79} \\
& \times \left(1.98 + \alpha_T\right)^{1.36} \beta_T^{2.14} \\
& \times \left(\beta_T^{1.53} + 1.87\,\alpha_T - 0.16\right)^{-1.33}.
\end{aligned}
\tag{3.64}
$$

Appendix C contains the description of the multidimensional weighted least-squares method, which has been used for deriving this fit, as well as the analysis of different tested models.

For the entire range of fitting variables, i.e. $10 < T_{e_0} < 100$ keV, $4 \times 10^2 < p_{a_0} < 1 \times 10^4$, $1 < \kappa < 2.5$, $0 < \alpha_n < 2$, $0 < \alpha_T < 8$, and $1 < \beta_T < 8$, the resulting RMSE is found to be 5.8%. Fig. 3.23 illustrates the agreement of the fit with the complete computation using Eq. (3.60) for different temperature subsets.
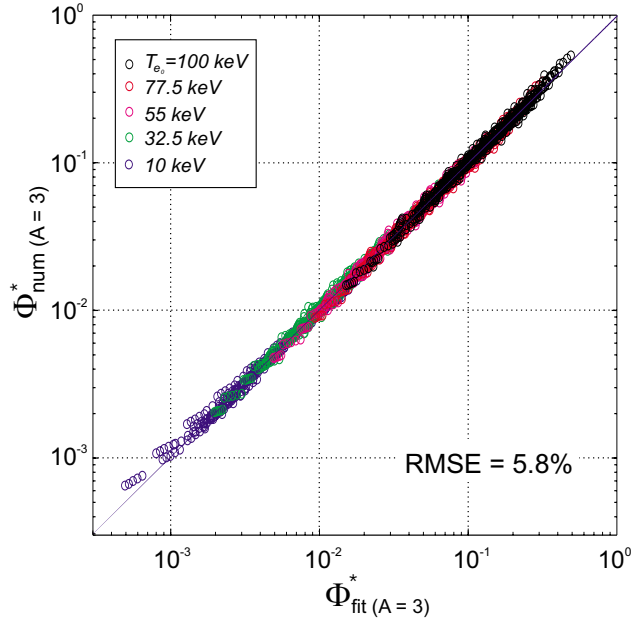

Figure 3.23: $\Phi^*_{\mathrm{num}\ (A=3)}$ parameter versus the proposed fit $\Phi^*_{\mathrm{fit}\ (A=3)}$ for the principal dataset.

The distribution of regression residuals is consistent with a normal distribution of standard deviation $\sigma = $ RMSE, as seen in Fig. 3.24. On the ordinate of this graph, we have the number of residuals n_{ε_i} which have a value within the interval $\varepsilon_i \pm \Delta H/2$ normalized both to the box width ΔH and to the total number of data n_{data}.
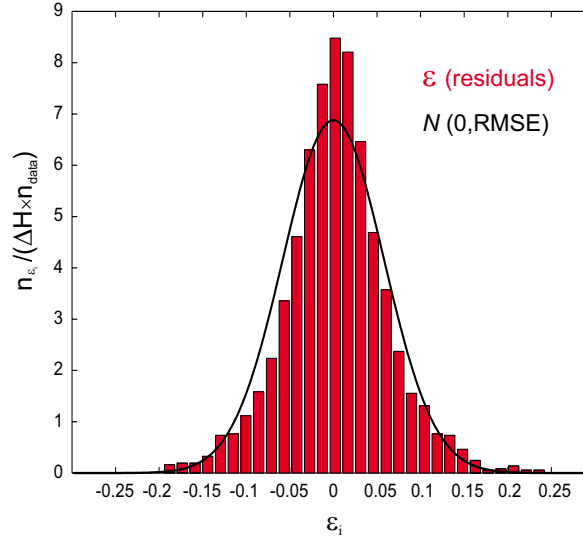
Figure 3.24: Distribution of regression residuals represented by red boxes, and the normal distribution $N\left(0, \text{RMSE}\right)$ represented by the black curve.

In order to take into account aspect ratios different from 3, a correction factor G is introduced:

$$\Phi^*_{\text{fit}} = \Phi^*_{\text{fit } (A=3)} G\left(A\right). \tag{3.65}$$

As seen in Fig. 3.19, the power loss due to synchrotron radiation grows as the aspect ratio decreases, when a is kept constant (in this case, $\Phi^*_{\text{fit } (A=3)}$ is also constant for varying values of A). At high aspect ratios ($A > 6$), although P_{syn} increases with R, the normalized synchrotron loss (Φ^* parameter) saturates. This is due to the fact that the magnetic field inhomogeneity vanishes for large A. For the above reason an exponential form is proposed for the G correction factor:

$$G\left(A\right) = 0.93 \left[1 + 0.85 \exp\left(-0.82\,A\right)\right], \tag{3.66}$$

giving an RMSE of 6.2% with respect to a secondary dataset consisting of 640 complete computations of Eq. (3.60), for the same range of fitting variables as the principal dataset and for an aspect ratio interval $1.5 < A < 15$.

Using engineering plasma parameters, Eq. (3.65) leads to a practical formula for the synchrotron power loss (expressed in MW) including the estimation of wall

reflections proposed in Ref. [Tru79]:

$$P_{\text{syn}}\,(\text{MW}) = 3.84 \times 10^{-8}\,(1-r)^{1/2}\,R\,a^{1.38}\kappa^{0.79}$$
$$\times\,B_{t_0}^{2.62}n_{e_0(20)}^{0.38}T_{e_0}\,(16 + T_{e_0})^{2.61}$$
$$\times\,\left(1 + 0.12\frac{T_{e_0}}{p_{a_0}^{0.41}}\right)^{-1.51}K\,(\alpha_n, \alpha_T, \beta_T)\,G\,(A) \qquad (3.67)$$

with

$$p_{a_0} = 6.04 \times 10^3 \frac{a n_{e_0(20)}}{B_{t_0}},$$

where units are m for the major and minor radii R and a, T for the toroidal magnetic field B_{t_0}, $10^{20}\,\text{m}^{-3}$ for the central density $n_{e_0(20)}$, and keV for the central electron temperature T_{e_0}, while K and G are given in Eqs (3.64) and (3.66), respectively.

The accuracy of the proposed fit for the fast calculation of synchrotron losses in system studies is acceptable considering the uncertainties in the other terms of the thermal equilibrium equation (Eq. (2.1)). For example, the RMSE for the IPB98(y,2) ELMy H-mode thermal confinement scaling [IPB99] is 15.6%. It should also be noted that the wall reflection coefficient for the synchrotron radiation is poorly known.

In Fig. 3.25 we compare the behaviour of the numerical transparency factor parameter, the proposed fit (Eq. (3.65)) and the FMGG fit when varying the values of the central electron temperature T_{e_0}, the central dimensionless parameter p_{a_0}, the vertical elongation κ, the density peaking factor α_n, the temperature peaking factors α_T and β_T, and the aspect ratio A (keeping a constant). In each case, the non-varying dimensionless variables are taken from the European Commercial Reactor nominal values. For all variables, the proposed fit shows a very good agreement with the complete calculation. We also note that the FMGG fit is not accurate at very high temperatures, does not describe precisely the aspect ratio dependence (as already mentioned in Section 4), and of course does not include the β_T dependence.

The results in Fig. 3.25 confirm the strong increase of the synchrotron losses with the central electron temperature (a), the drastic decrease with the p_{a_0} parameter (b), and the high sensitivity of synchrotron losses to the temperature peaking parameters α_T (e) and β_T (f). Let us also note the factor 2 of increase between circular and very elongated plasmas ($\kappa = 2.5$), as seen in Fig. 3.25(c).

3.9 Summary

A complete formulation of synchrotron radiation losses without wall reflections has been performed for realistic plasma conditions, including a toroidal geometry with arbitrary aspect ratio, arbitrary shapes for density and temperature profiles, and
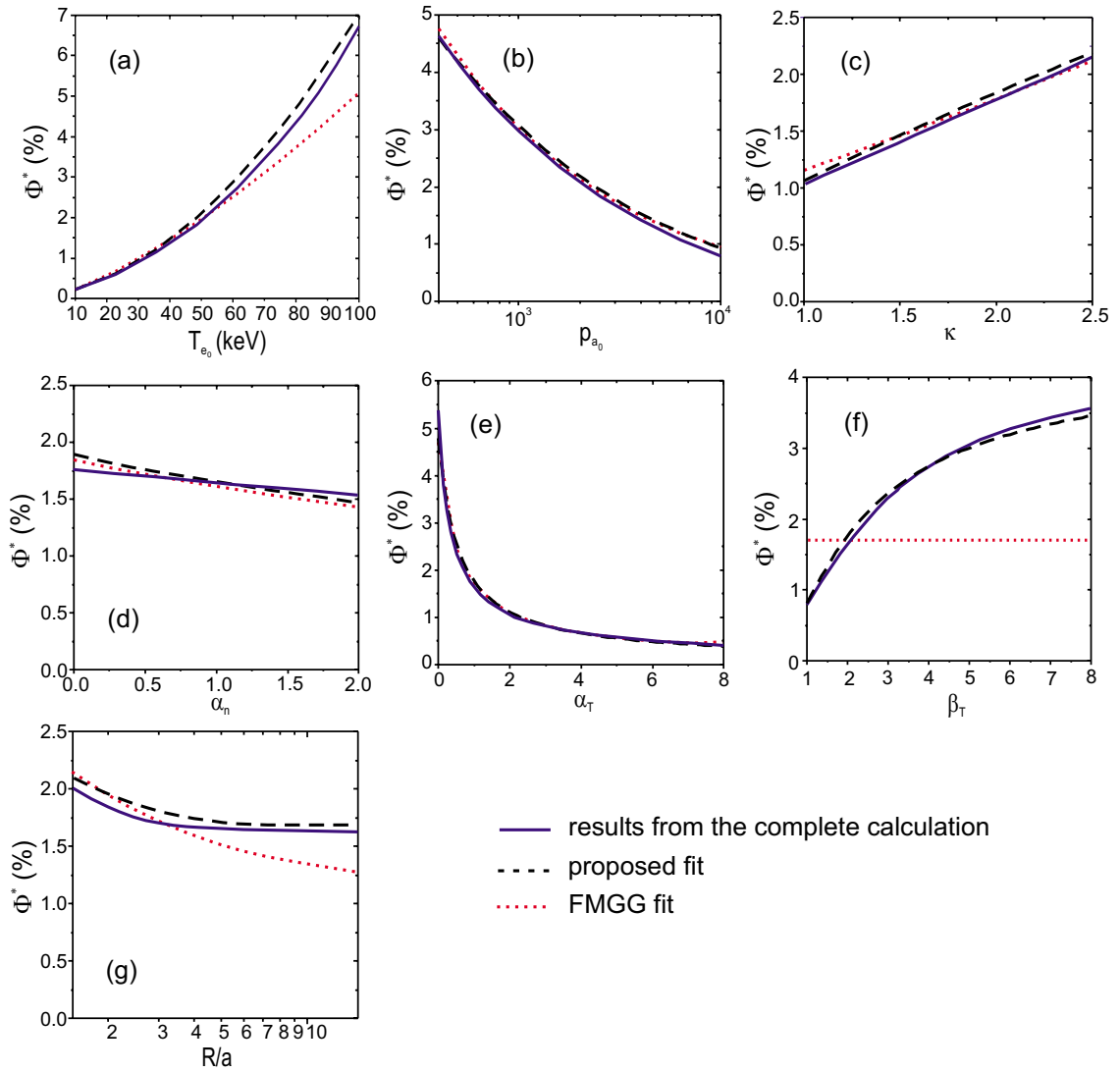
Figure 3.25: Comparison of the Φ^* parameter calculated numerically, calculated with the proposed fit (Eq. (3.65)) and calculated with the FMGG expression when varying the values of (a) the central electron temperature T_{e_0}, (b) central opacity factor p_{a_0}, (c) vertical elongation κ, (d) density peaking factor α_n, temperature peaking factors (e) α_T and (f) β_T, and (g) aspect ratio A.

a quasi-exact calculation of the plasma self-absorption. Trubnikov's approximate method for the calculation of the absorption coefficients, which gives much faster calculations, has been shown to introduce non-negligible errors.

The case of cylindrical homogeneous plasmas with circular cross-section has been analysed using Trubnikov's approximate method for the calculation of the absorption coefficients. In this case, we obtain an acceptable agreement between our numerical results and those reported by Trubnikov. When an elliptical cross-section is considered, it is found that the synchrotron loss dependences on the temperature and opacity factor are fairly independent from the value of the elongation. This behaviour is also observed for toroidal plasmas.

For generalized parabolic profiles, when all toroidal effects are taken into account, and when we use the quasi-exact calculation of the absorption coefficients, our results differ significantly from those obtained using the FMGG fit, for aspect ratios differing from 3.5. The agreement of this fit with our formulation, for aspect ratios of about 3.5, is explained by a compensation of the errors introduced by the description simplified phenomena and geometry, and by the approximations made for the calculation of the plasma self-absorption.

For profiles in which high temperatures are maintained up to a non-central layer (which is the case of ITB regimes), we see a strong enhancement of synchrotron losses (around 20-40%) with respect to the result corresponding to the best generalized parabolic fit. The strong effect of the temperature profile shape on synchrotron losses has been explained using the spatial density of the synchrotron power loss in terms of emission, which shows the plasma region that participates the most to the global synchrotron losses as a competition between emission and absorption processes.

In Chapter 6, we illustrate that synchrotron losses become significant in the advanced high temperature plasmas envisaged for a continuous D-T tokamak reactor. Considering the quantitative importance of the above effects, which are not included in present approximate expressions, and the magnitude of synchrotron losses in the thermal balance of a D-T tokamak reactor plasma, we propose a new fit for the fast calculation of this quantity. This fit gives a good accuracy for the entire range of plasma parameters of interest for the thermonuclear energy problem.

The remaining issue in the study of synchrotron losses is the rigorous analysis of wall reflections, which cannot be carried out in toroidal geometry using the formulation presented here. To treat this problem, a Monte Carlo approach must be developed, which would also allow the investigation of the energy redistribution on the plasma profile.